International Journal of Greenhouse Gas Control 7 (2012) 244–260

Contents lists available at SciVerse ScienceDirect

International Journal of Greenhouse Gas Control

journal homepage: www.elsevier.com/locate/ijggc

Assessing the monitorability of CO_2 saturation in subsurface saline aquifers

Arash JafarGandomi*, Andrew Curtis

School of GeoSciences, University of Edinburgh, King's Buildings, Edinburgh EH9 3JW, United Kingdom

ARTICLE INFO

Article history:
Received 3 June 2011
Received in revised form 12 October 2011
Accepted 30 October 2011
Available online 30 November 2011

Keywords:
Geophysical monitoring
Reservoir characterization
CO_2 storage
Information theory
Markov-chain Monte Carlo inversion
Survey design

ABSTRACT

We propose a method to assess the geophysical monitorability of petrophysical parameters (in this case CO_2 saturation) in subsurface geological reservoirs. The approach is based on measuring and inverting up to six geophysical parameters: P- and S-wave impedances and quality factors (1/attenuation), density and electrical resistivity. We use Shannon's information measure to quantify the information obtained from the inversion of different combinations of geophysical parameters. We thus develop a generic approach to assess the joint monitorability of supercritical CO_2 saturation when CO_2 is stored in subsurface reservoirs. Uncertainty analysis shows that expected information is in general nonlinearly related to the level of a priori or measurement uncertainty in the geophysical and petrophysical parameters, to the true CO_2 saturation, and also to the measurement frequency in the case of seismic measurements. Prior uncertainties in petrophysical parameters such as porosity have a significant effect on the monitorability, highlighting the need for accurate benchmark (pre-injection) measurements and reservoir characterization in the case of time-lapse (4D) monitoring. We show that estimates of P-wave seismic attenuation contribute most to the overall information obtained, and that in principle the joint application of different geophysical methods can significantly improve monitorability. We applied the approach to assess the monitorability of the CO_2 saturation after 10 years of simulated injection into a saline aquifer reservoir in the near-shore UK North Sea. Application of the approach to design optimal data combinations for hydrocarbon saturation assessment and monitoring is straightforward.

1. Introduction

The process of capturing carbon dioxide (CO_2) and injecting it into deep subsurface saline aquifers is potentially an important method to reduce atmospheric emissions of CO_2 from large point-source emitters such as power stations. In order to detect, and reduce the corresponding risks posed by leakage, comprehensive long-term monitoring is likely to be required. Any geophysical monitoring technique employed must be able to detect where a certain minimum threshold CO_2 saturation and volume has been exceeded within a subsurface reservoir (for development and measurement purposes), or after leakage into the overburden. The required characteristic volume and accuracy threshold define the minimum threshold of detectability and monitorability of dynamically propagating CO_2, and hence the level of risk mitigation possible using geophysical technique.

Several studies on geophysical monitoring of subsurface CO_2 storage have been published recently (e.g., Arts et al., 2004; Alnes et al., 2008; Daley et al., 2008; Gasperikova and Hoversten, 2008; Yordkayhun et al., 2009). Most of these focus on detecting the CO_2 plume and its spatial extent. There are also several laboratory studies that quantify the effect of CO_2 on the petrophysical properties of rocks [e.g., Xue and Ohsumi, 2004; Xue and Lei, 2006; Siggins, 2006; Shi et al., 2007; Lei and Xue, 2009; Xue et al., 2009). However, a quantitative investigation of the geophysical monitorability of sequestered CO_2 stored in geological formations from a petrophysical point of view is lacking.

The process of estimation of reservoir parameters such as CO_2 saturation (S_{CO_2}) generally consists of a series of geophysical and petrophysical inversions (Fig. 1). Recorded geophysical (e.g., seismic and electromagnetic) data first undergo a geophysical inversion in order to estimate the subsurface spatial distribution of what we call *geophysical parameters* (shorthand for parameters that are directly inferable from geophysical data e.g., P- and S-wave impedances I_P and I_S respectively, density ρ, resistivity r, etc.). These estimates are subsequently inverted in a petrophysical inversion to estimate petrophysical parameters (e.g., porosity, clay content, permeability, fluid saturations like S_{CO_2}, etc. – generally, the properties used in petrophysical models to estimate geophysical parameters). In practice, the observed data and the associated measurement uncertainty are strongly dependent on the observational conditions, which are ultimately reflected in the uncertainties of estimated geophysical parameters. In this paper, in the absence of real field measurements and to keep the generality and efficiency of the approach, we incorporate the concerns about

* Corresponding author. Present address: Lancaster Environment Centre, Lancaster University, Lancaster LA1 4YQ, United Kingdom. fax: +44 131 668 3184.
E-mail address: a.jafargandomi@lancaster.ac.uk (A. JafarGandomi).

1750-5836/$ – see front matter © 2011 Elsevier Ltd. All rights reserved.
doi:10.1016/j.ijggc.2011.10.015

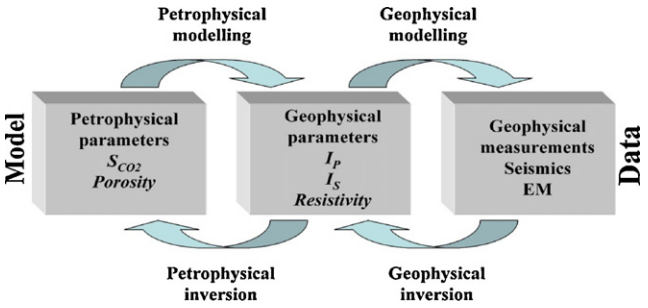

Fig. 1. Two-stage computational modelling and inversion operations required to estimate petrophysical and geophysical parameters from geophysical measurements (data).

observational conditions by introducing degrees of freedom to the level of uncertainties in the estimated geophysical parameters. Therefore, we focus on the petrophysical inversion and show how to use information about petrophysical parameters to assess their geophysical monitorability.

To fulfil the monitoring objectives there must be sufficient resolution and uncertainty reduction in petrophysical and fluid parameter estimates. We use a Monte Carlo inversion approach to describe reservoir parameters and their associated uncertainties (e.g., Bachrach, 2006; Larsen et al., 2006; Spikes et al., 2007; Bosch et al., 2007; Chen and Dickens, 2009). To quantify the information content of the so-called posterior probability distributions, we use Shannon's entropy (Shannon, 1948), which is an appropriate single parameter to describe probability distributions even when they are multimodal or highly skewed.

The main objective of this paper is to assess the applicability of different geophysical parameters individually and in combination with each other, to reduce uncertainties in reservoir parameter estimates. Reducing uncertainty requires elaborate data gathering, processing and inversion workflows. Optimal experimental and data processing designs may be used to improve these uncertainties. Optimal design theory is applied to both linear and nonlinear geophysical problems (Curtis, 2004a,b) such as seismic tomography (Curtis, 1999a,b; Maurer et al., 2009; Ajo-Franklin, 2009), amplitude variation with offset/angle survey and processing (van den Berg et al., 2003; Coles and Curtis, 2010; Guest and Curtis, 2009, 2010, 2011) earthquake or microcosmic location surveys (Curtis et al., 2004; Winterfors and Curtis, 2008) and electric and electromagnetic surveys (Maurer and Boerner, 1998; Maurer et al., 2000; Stummer et al., 2002a,b, 2004; Oldenborger et al., 2007). A review of the recent advances in survey design is given in Maurer et al. (2010). The choice of method to use to design experiments depends greatly on how one can measure the information about model parameters that is expected to be gleaned from the data. Here we draw from experimental design and information theory to develop methods to estimate information for key petrophysical parameters that assist in operational decision-making for subsurface CO_2 storage, given various qualities of geophysical parameter estimates. This in turn identifies key contributions to uncertainty and allows an appropriate selection of geophysical monitoring technique(s) to reduce overall uncertainty on petrophysical parameters.

Assessing expected uncertainties is a particular challenge for CO_2 storage in extensive saline aquifers in the UK North Sea where, in contrast to the hydrocarbon reservoirs, very little data is available (e.g., Haszeldine, 2009). In such cases, geophysical monitorability assessments are relevant for reservoir characterization both before and after drilling. We use a real example of near-shore aquifer reservoir analogues to demonstrate our method.

In the next section, we present the general theoretical background and methods applied. Then the methodology is adapted to a specific UK North Sea saline aquifer, and we asses the monitorability of the aquifer reservoir after 10 years of hypothetical (simulated) CO_2 injection. Finally, the results are discussed and conclusions drawn.

2. Theory and method

In this section we explain the theory and methodology to assess the monitor ability of reservoir parameters such as S_{CO_2} and porosity. Since in usual survey design situations little or no geophysical data has yet been acquired, the methods must assess *expected* post-survey parameter information.

2.1. Bayesian inversion

We analyses uncertainties in geophysical and petrophysical parameters within a Bayesian framework. In this framework the solution to an inverse problem is represented by a posterior (post-inversion) probability distribution function (pdf), $\sigma(\mathbf{m})$, over the model parameters $\mathbf{m}$ (e.g., Tarantola, 2005). The posterior pdf is related to the so-called prior pdf $\rho(\mathbf{m})$ which represents pre-inversion knowledge about parameters $\mathbf{m}$, through

$$\sigma(\mathbf{m}) = CL(\mathbf{m})\rho(\mathbf{m}) \tag{1}$$

where C is a constant and $L(\mathbf{m})$ is the likelihood function which describes how well the synthetic or modelled data corresponding to each model $\mathbf{m}$ match the recorded data, and here is defined to be a multivariate Gaussian in the difference between observed data d^i_{obs} and synthetic data $d^i(\mathbf{m})$:

$$L^i(\mathbf{m}) = \frac{1}{\sqrt{2\pi\left|\sum\right|}} \exp\left(-\frac{1}{2}\boldsymbol{\varepsilon}^T \sum^{-1} \boldsymbol{\varepsilon}\right), \tag{2}$$

where $\sum$ is the covariance matrix and $\boldsymbol{\varepsilon}$ is the vector difference between observed data and synthetic data. We assume here that data are independent and hence the covariance matrix is diagonal with elements σ^i for datum d^i where superscript $i = 1,\ldots,6$ refers to each of P- and S-wave impedances and quality factors (reciprocal of attenuation), bulk density and electrical resistivity, I_P, I_S, Q_P, Q_S, ρ, r, respectively.

Below we will generate posterior pdfs corresponding to specific potential recorded data sets using a Markov-chain Monte Carlo sampling method. Sambridge and Mosegaard (2002) reviewed the theory and application of Monte Carlo methods in geophysical inverse problems, and recently Monte Carlo inversion has been used in several studies to describe hydrocarbon reservoir parameters (e.g., Bosch et al., 2007; Chen et al., 2007; Chen and Dickens, 2009). To obtain Monte Carlo samples of the posterior pdf we use the Metropolis method (Metropolis et al., 1953) which is a Markov-chain Monte Carlo algorithm. According to the Metropolis algorithm the probability of visiting a future point in model space depends only on the current point and not on the previously visited points – this is the co-called Markov property. We sequentially update a set of estimates of the petrophysical parameters (e.g., S_{CO_2}, porosity, clay content described by vector $\mathbf{m}$) using the following steps:

- Start with initial values for $\mathbf{m}_j$ (S_{CO_2}, porosity, and clay content) and calculate corresponding geophysical parameters $\mathbf{d}(\mathbf{m}_j)$ by forward petrophysical modelling. Calculate the geophysical likelihood $L(\mathbf{m}_j)$.
- Define a new candidate parameter vector $\mathbf{m}_{j+1}$ by randomly selecting candidate petrophysical values from the prior

distribution. Calculate the corresponding geophysical parameters $\mathbf{d}(\mathbf{m}_{j+1})$ and likelihood $L(\mathbf{m}_{j+1})$.
- Use the Metropolis rule to accept or reject the new candidate model by calculating the ratio of the current and candidate likelihoods $L(\mathbf{m}_{j+1})/L(\mathbf{m}_j)$. The acceptance probability is

$$P = \min\left[1, \frac{L(\mathbf{m}_{j+1})}{L(\mathbf{m}_j)}\right]$$

- If the candidate model configuration is rejected, the current model remains for the next iteration, otherwise $\mathbf{m}_{j+1}$ is accepted as the next model sample.
- Repeat Steps 2 and 3 until the required number of samples in the set $S = \{\mathbf{m}_1, \mathbf{m}_2, \ldots, \mathbf{m}_N\}$ is obtained.

The set S contains a set of samples that approximate samples of the posterior pdf, particularly if only every kth sample from the set is used where k is a constant that is of the order of the number of parameters in $\mathbf{m}$. By calculating the sample density in S, we obtain an estimate of the posterior pdf $\sigma(\mathbf{m})$ for any new measured data $\mathbf{d}_{obs}$.

2.2. Information quantification

The state of knowledge about any random or uncertain parameter that is described by a pdf may be quantified by using an information measure (Lindley, 1956). In designing any CO_2 monitoring strategy we wish to maximize the information that is expected to be obtained about the parameter S_{CO_2}. Ignoring cost and logistics for the moment, Lomax et al. (2009) and Maurer et al. (2010) introduced an objective function in the following form

$$J(\xi) = E_{\mathbf{m}}\left\{I\left[\sigma(\mathbf{m}); \xi, \mathbf{m}\right]\right\}, \tag{3}$$

where ξ is a vector describing the survey design (e.g., the number, types and location of sensors and sources to be used), $I[\sigma(\mathbf{m});\xi,\mathbf{m}]$ is a measure of the information contained in the resulting posterior pdf $\sigma(\mathbf{m})$ obtained for design ξ when the true model parameters are given by $\mathbf{m}$, and the statistical expectation operator $E_{\mathbf{m}}$ averages I over the prior distribution $\rho(\mathbf{m})$ of all possible values for the true parameter values $\mathbf{m}$.

Shannon (1948) introduced a unique, linear measure of information represented by any pdf $f(\mathbf{x})$ by

$$I[f(\mathbf{x})] = -Ent(\mathbf{x}) + c = \int_{\mathbf{x}} f(\mathbf{x}) \log[f(\mathbf{x})]\ d\mathbf{x} + c \tag{4}$$

Here I is the information measure as defined by Shannon (1948), Ent is the entropy function defined in the right hand side, $f(\mathbf{x})$ is the pdf of the random variable $\mathbf{x}$, and c is a constant. Similarly, the information represented by any joint pdf $f(\mathbf{x},\mathbf{y})$ is

$$I[f(\mathbf{x},\mathbf{y})] = \int_{\mathbf{x},\mathbf{y}} f(\mathbf{x},\mathbf{y}) \log[f(\mathbf{x},\mathbf{y})]\ d\mathbf{x}d\mathbf{y} + c \tag{5}$$

The unit of information depends on the base of the logarithm in equations (4 and 5). The corresponding units for logarithm bases 10, Euler's number e, and 2 are *dit*, *nat* and *bit*, respectively. From hereon, we use base-e logarithm for estimation of information and the information unit is *nat*. Generally speaking, information about a parameter is maximized when its pdf constrains its possible ranges of values most tightly (Lindley, 1956). Shannon's entropy has been widely used in experimental design theory and applications (e.g., Sebastiani and Wynn, 2000; Zidek et al., 2000; van den Berg et al., 2003; Curtis, 2004a,b; Krause et al., 2008; Guest and Curtis, 2009, 2010; JafarGandomi and Curtis, 2010).

Calculation of Shannon's entropy is a significant issue from a computational point of view. Ahmed and Gokhale (1989) showed that Shannon's entropy of a multivariate Gaussian distribution is $Ent = \mathrm{Log}\left[(2\pi\, e)^N \left|\Sigma\right|\right]/2$ where N indicates the number of variables. Shannon's entropy of a uniform distribution is $\mathrm{Log}\left|b-a\right|$ where a and b are lower and upper bounds of the distribution. Cover and Thomas (2006) gave an analytical solution for equation (4) for a particular set of pdf's. However, uncertainties in many real world problems cannot be represented with any single one of these analytical pdf's. Gaussian mixture densities (Maz'ya and Schmidt, 1996) which are constructed by weighted superposition of a number of single Gaussian distribution are often used to represent non-Gaussian densities. Given a sufficient number of components, they can approximate any smooth function to any desired level of accuracy. Several approximations have been proposed to calculate the entropy of Gaussian mixtures effectively (e.g., Huber et al., 2008). Another approximation that can be demonstrated to converge to the true entropy relies on random sampling methods such as Monte Carlo that we use in this paper. In the following sections we estimate information in the posterior pdf to assess the quality of information about parameters $\mathbf{m}$ using,

$$I[\sigma(\mathbf{m})] = c + \int_{\mathbf{m}} \sigma(\mathbf{m}) \log[\sigma(\mathbf{m})]\ d\mathbf{m} \approx c + \sum_{j=1}^{n}\sum_{i=1}^{m} \log\left[\sigma\left(\mathbf{m}_{i,j}\right)\right]\ \sigma\left(\mathbf{m}_{i,j}\right) \tag{6}$$

corresponding to equation (5), where I is Shannon's information, $i = 1,2,\ldots, m$ and $j = 1,2,\ldots, n$ are the bin numbers within a finely gridded or discretised model space, $\sigma(\mathbf{m}_{i,j})$ is the joint posterior pdf of S_{CO_2} and porosity and c is a constant which we will ignore in this paper since we compare relative values of I rather than absolute values. To calculate the information we first calculate a grid of local histograms of the samples of the posterior distribution around each of a grid of parameter values $\mathbf{m}_{i,j}$ distributed throughout model space, then normalise the sum of all histograms to have unit volume, where after the set of histograms represents a discretised numerical approximation to the posterior pdf. The set of values $\sigma(\mathbf{m}_{i,j})$ used in equation (6) are the values of these normalised histograms.

3. Geophysical properties of CO_2 bearing rocks

The geophysical parameters of rock (i.e. P- and S-wave velocities/impedances and attenuations, bulk density and electrical resistivity) pre- and post-CO_2 injection depend on the mineralogical composition, porosity, pore fluid content (including the saturation of CO_2), and in situ pressure and temperature of the rock, as well as on the physical parameters of the injected CO_2. There are several laboratory studies that quantify the effect of CO_2 on the petrophysical parameters of rocks (e.g., Xue and Ohsumi, 2004; Xue and Lei, 2006; Siggins, 2006; Shi et al., 2007; Lei and Xue, 2009). In this section we construct a petrophysical model based on existing models to describe the effect of CO_2 saturation on the geophysical parameters. In the following section we use this model for Monte Carlo inversion of geophysical parameters.

3.1. Petrophysical model

In partially saturated rocks the bulk modulus depends not only on the degree of saturation, but also on the mesoscopic and microscopic characterization of saturation. Patchy saturation and uniform saturation are considered to be extreme cases of saturation distributions (Mavko et al., 1998). Saturation type has a direct effect

Table 1
Material parameters of clay bearing sandstone and the pore fluids it contains.

Sand	Bulk modulus	39 GPa
	Shear modulus	33 GPa
	Density	2650 km/m^3
	Average particle diameter	100 μm
Clay	Bulk modulus	25 GPa
	Shear modulus	9 GPa
	Density	2650 km/m^3
	Average particle diameter	2 μm
Brine	Bulk modulus	2.4 GPa
	Density	1030 kg/m^3
	Viscosity	1.798 cP
CO_2	Bulk modulus	0.186 GPa
	Density	786 kg/m^3
	Viscosity	0.06 cP
Gas	Bulk modulus	0.01 GPa
	Density	100 kg/m^3
	Viscosity	0.02 cP

on the bulk modulus of the effective fluid (in this case a composite of CO_2 and brine) that depends on the moduli of the constituents and their spatial distribution. Recent studies have shown that intrinsic attenuation at seismic frequencies (1–10,000 Hz) in porous media is mainly due to wave-induced fluid flow at the mesoscopic-scale – larger than the pores but smaller than the wavelength (Pride et al., 2004). Furthermore, Lei and Xue (2009) have shown that intrinsic attenuation (in a porous rock of relatively lower permeability) at ultrasonic frequencies up to a few 100 kHz is also due to wave-induced fluid flow at the mesoscopic scale. Mesoscopic-scale attenuation was first modelled by White (1975) and White et al. (1975). Dutta and Seriff (1979) reformulated this model by using Biot's theory of poroelasticity (Biot, 1956) and confirmed the accuracy of White's model. However, they identified a mistake in White (1975) formulations, where the P-wave modulus was used instead of the bulk modulus to derive the complex bulk modulus. Hereon, we use the corrected White's model.

In addition to mesoscopis-scale attenuation, Biot and squirt flow are the other known phenomena responsible for wave attenuation at high frequency. The model proposed by Pham et al. (2002) contains both Biot and squirt flow effects. Their model calculates wave velocities and attenuation of clay-bearing sandstones as a function of pore pressure, frequency and partial saturation. We combine White's (1975) model with Pham et al.'s (2002) model by adjusting the matrix bulk modulus of the latter with the frequency dependent bulk modulus of the former (see Appendix A).

We compare the calculated P-wave velocity and attenuation of White (1975), Pham et al. (2002), and combined models with respect to frequency for a rock sample with 22.6% porosity, no clay content, 50% water saturation and 50% gas saturation (Fig. 2). In this example the effective pressure is 40 MPa and the viscoelasticity of the solid frame is neglected, however this constraint is relaxed in the next sections. We assume patches of the same size by setting the period of White's layered model $d_1 + d_2 = 20$ cm where d_1 and d_2 indicate thicknesses of the layers in hypothetical porous media saturated with brine and gas, respectively (see Appendix A for more details about White's model). The corresponding material parameters are given in Table 1. Two attenuation peaks at low and high frequencies in Fig. 2 correspond to mesoscopic-scale and squirt flow losses, respectively. While either of the White (1975) and Pham et al. (2002) models represent one of these peaks, the combined model successfully represents both.

The resistivity of the rock can be predicted using the empirical relation known as Archie's law (Archie, 1942). Even though Archie's law has been used widely for describing electrical resistivity of rocks, it is strictly valid only for homogenous and water-wet rocks

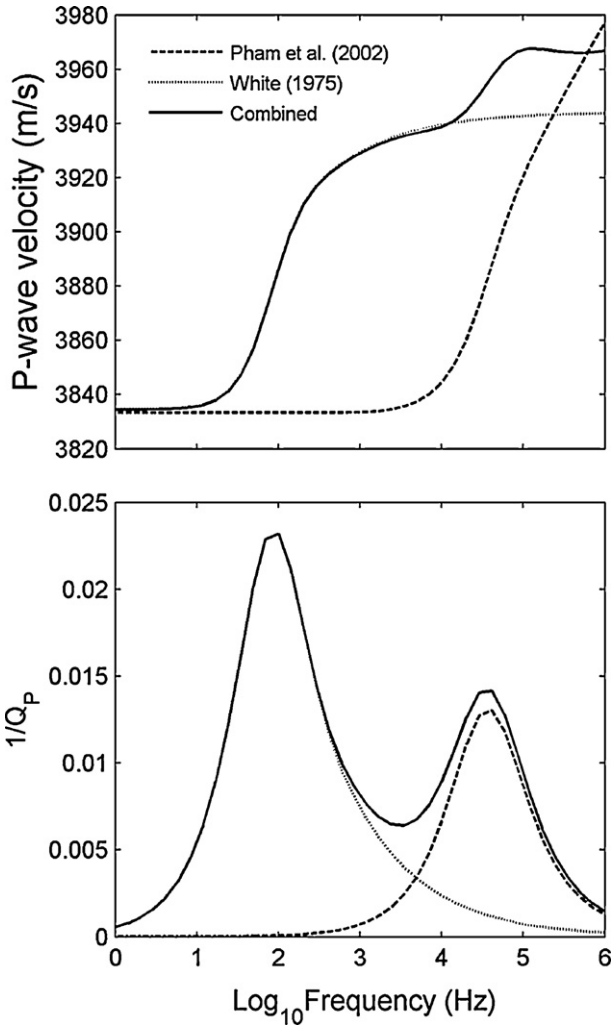

Fig. 2. Calculated phase velocity (a) and attenuation (b) curves corresponding to the sandstone with 50% water saturation with White (1975) (dotted line), Pham et al. (2002) (dashed line) and combined models (solid line).

(e.g., Toumelin and Torres-Verdín, 2008), and introducing clay content into the model is also not straightforward. Pride (1994) derived the macroscopic (dimensions of the grains much smaller than the wavelength of the applied electromagnetic disturbances) governing equations for coupled electromagnetics of porous media. The main advantage of this model for our purpose is that introducing different sand and clay contents into the model is straightforward and in accordance with the Pham et al. (2002) model for elastic parameters (a review of the Pride (1994) model is given in Appendix A). We estimate the coefficients of the petrophysical models by fitting the predictions to the laboratory measurements of representative reservoir rock samples from the North Sea reservoir rock and they remain unchanged throughout the rest of this paper (Table 2).

Table 2
Values of parameters used in the petrophysical model.

Parameter	Value
A (equation (A-4))	3.03–3.16
B (equation (A-9))	15
ϕ_P (equation (A-9))	0.035
S_{wi} (equation (A-10))	0.2
S_{gi} (equation (A-11))	0.1
m_w (equation (A-10))	1.1
m_g (equation (A-11))	1.5

4. Resolution of petrophysical parameters

In this section we show how to assess the expected monitorability of S_{CO_2} in any target formation from Monte Carlo inversion of P- and S-wave impedances and quality factors, density, and electrical resistivity (I_P, I_S, Q_P, Q_S, ρ, r, respectively). In a nutshell, given a particular monitoring method or strategy for each of a range of petrophysical models sampled from the prior pdf, we forward model the corresponding expected values of geophysical parameters that would be measured. Then, while accounting for expected uncertainties, we invert the geophysical parameter estimates for the posterior distribution $\sigma(\mathbf{m})$ of the petrophysical model $\mathbf{m}$. This estimate of $\sigma(\mathbf{m})$ then describes the expected post-survey state of information about the petrophysical model, so finally, we quantify the uncertainty in joint S_{CO_2} and porosity estimates given that particular monitoring method or strategy using the information measure in equation (6). This workflow is shown schematically in Fig. 3.

We begin by calculating geophysical parameters corresponding to are presentative reservoir rock sample with 22.6% porosity and 5% clay content for a range of S_{CO_2} (0–100%). We estimate the information in the joint posterior distributions of S_{CO_2} and porosity inverted from elastic parameter estimates at two frequencies of 30 Hz and 3000 Hz, representing seismic and sonic frequency ranges, respectively. From hereon, we show the information estimated for I_P, I_S, Q_P, and Q_S with $I\left(I_P^f\right)$, $I\left(I_S^f\right)$, $I\left(Q_P^f\right)$, and $I\left(Q_S^f\right)$ where superscript f = 30, 3000 indicates low (30 Hz) or high (3000 Hz) frequencies, respectively. We assume uniform prior pdfs for S_{CO_2}, porosity and clay content in the ranges 0–100%, 0–40% and 0–50%, respectively, which may represent a reservoir that has not been characterized before monitoring. We randomly sample the prior distributions 10,000 times and use the Metropolis algorithm to sub-select samples of the posterior distributions for 10 discrete values of true S_{CO_2}. The information is calculated for 2%, 4%, 6% and 8% uncertainties in geophysical parameter estimates.

Figs. 4 and 5 show that information obtained is in general nonlinearly related to the true value of the petrophysical parameters, frequency of measurement, and uncertainty in estimated geophysical parameter. For comparison, the minimum possible information about petrophysical parameters is −8.294 which corresponds to the prior uniform joint pdf for S_{CO_2} and porosity in the ranges 0–100% and 0–40%, respectively. For the same uncertainties in estimated parameters, $I\left(Q_P^{30}\right)$ presents the highest value and the highest sensitivity to true S_{CO_2}. As may be expected intuitively, $I\left(I_S^{30}\right)$ and $I\left(Q_S^{30}\right)$ show low values and very little sensitivity to true S_{CO_2} because shear wave propagation is dominantly sensitive to solid rock and grain properties, and, increasing uncertainty in geophysical parameter estimates reduces the obtained information.

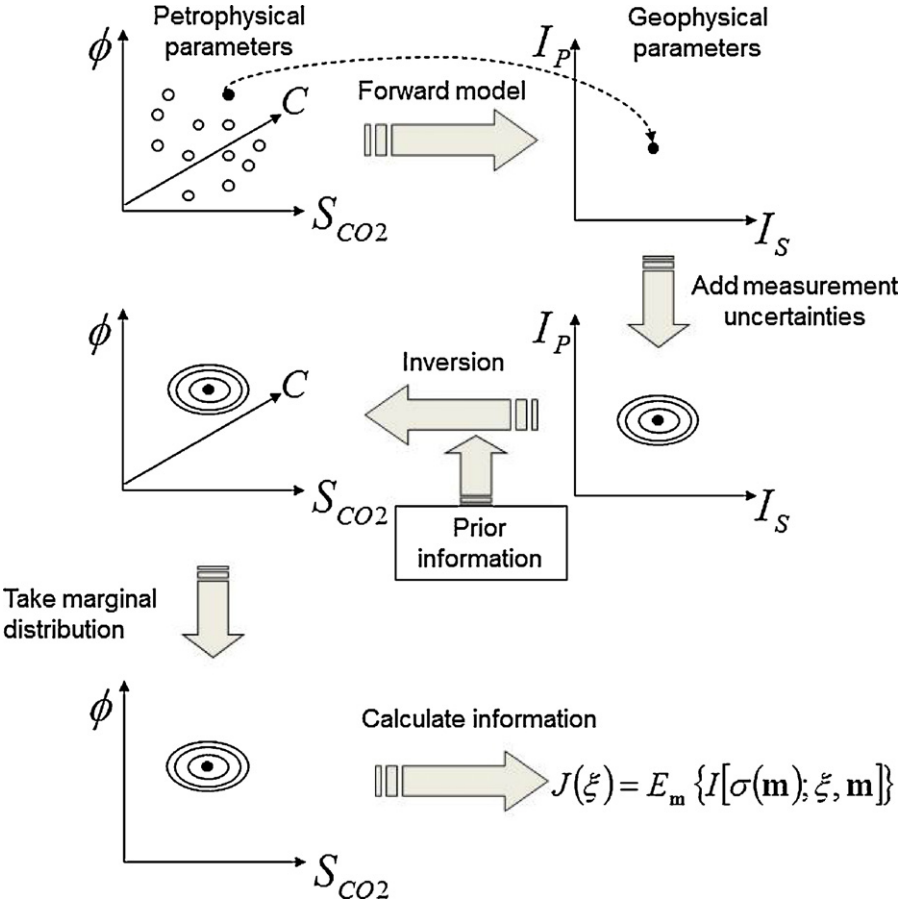

Fig. 3. Schematic workflow for assessing the expected information about petrophysical parameters in any target formation from a specific type of geophysical measurements. Each sample from the prior probability distribution over petrophysical model parameters (top-left) is forward modelled to give geophysical parameter values (top-right). Expected uncertainties in the geophysical parameters are added (middle-right), and these uncertain data are inverted while injecting relevant prior information to give the posterior distribution $\sigma(\mathbf{m})$ (middle-left). The marginal posterior distribution over relevant petrophysical parameters (lower-left) contains all information expected from these geophysical data, and the information value is calculated (lower-right). The whole process is repeated over all prior petrophysical model samples (top-left), and the average information value gives the expected information from that geophysical monitoring method or strategy.

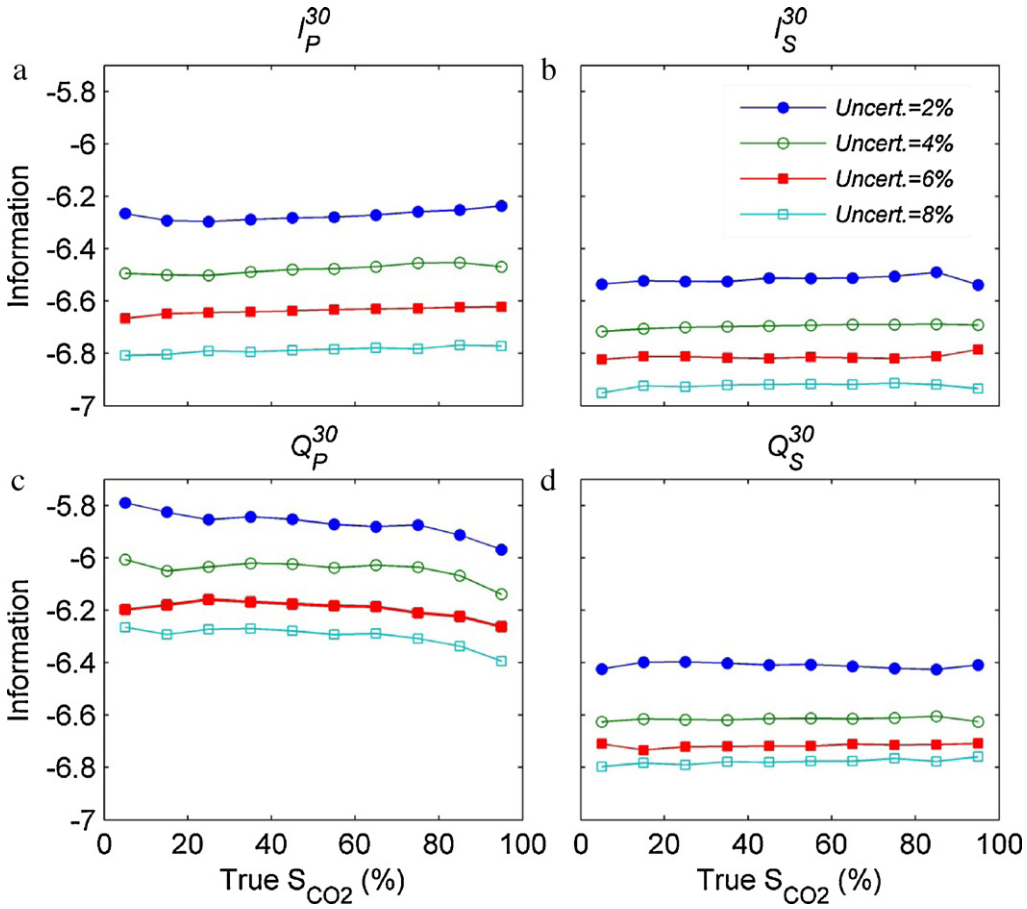

Fig. 4. Information values for different geophysical parameters as a function of true S_{CO_2}, inverted from (a) P-wave impedance I_P, (b) S-wave impedance I_S, (c) P-wave quality factor (reciprocal of attenuation) Q_P and (d) S-wave quality factor Q_S estimates, each with four different uncertainties, 2%, 4%, 6% and 8% at $f = 30$ Hz. The prior pdfs for S_{CO_2}, porosity and clay content are uniform in ranges 0–100%, 0–40% and 0–50%, respectively.

Comparisons of plots in Figs. 4 and 5 imply that frequency of measurements has little effect on $I\left(I_P^f\right)$ and $I\left(I_S^f\right)$, however, its impact on both $I\left(Q_P^f\right)$ and $I\left(Q_S^f\right)$ is significant. In particular, $I\left(Q_S^{3000}\right)$ is much greater than $I\left(Q_S^{30}\right)$. This indicates that while with low frequency methods such as reflection seismics, inversion of Q_S^f estimates with high uncertainty may not add much value to the obtained information, with higher frequency methods such as well-based methods (i.e., logging and cross-hole techniques) Q_S^f is more informative than I_P^f. The relatively high value of $I\left(Q_P^f\right)$ at both frequencies is due to the high sensitivity of Q_P^f to fluid flow: at low frequency mesoscopic-scale fluid flow and at high frequency Biot and squirt flow increases the information obtained from Q_P^f estimates.

Fig. 6 depicts similar information curves to those in Fig. 4 or Fig. 5, both for ρ and r [$I(\rho)$ and $I(r)$, respectively for which frequency of measurement is effectively irrelevant in geophysics]. Density provides less information than the other parameters about the reservoir parameters (Fig. 6a), however the bulk density change in the reservoir due to a large volume of injected CO_2 may be effectively detectable by using gravity measurements. Compared with the other geophysical parameters $I(r)$ curves in Fig. 6b present far higher values. This shows that electrical resistivity has the potential to aid S_{CO_2} monitoring, if it could be estimated reasonably accurately. The negligible sensitivity of electrical resistivity to the frequency of measurement over the frequency range of interest in geophysics may also be an advantage. Sensitivity of $I(r)$ to the uncertainties in resistivity estimates is particularly high for $S_{CO_2} > 50\%$ which is due to the logarithmic increase of resistivity with S_{CO_2}. Nevertheless, joint inversion of electrical resistivity and elastic parameters may significantly reduce the uncertainty in inversion results and improve monitoring capability.

Nonlinearity in the behaviour of information curves is due to the combination of two effects: hard boundary conditions at the highest and lowest values of S_{CO_2} (at 0% and 100%), and intrinsic variation of I_P, I_S, Q_P, and Q_S with respect to the saturation and frequency. Hard boundary conditions increase the information near to these boundaries because parameter uncertainty can only extend in one direction (away from the boundary) rather than two. This effect can be seen on $I\left(I_P^{30}\right)$ curves at the lowest and highest values of S_{CO_2}, and on the $I\left(Q_P^{30}\right)$ curve at the lowest S_{CO_2}. Curves of $I\left(Q_P^{3000}\right)$ show the coincidence of high sensitivity of Q_P^{3000} at the highest and the lowest S_{CO_2} together with the hard boundary conditions causing a significant increase in information. Essentially the fact that we cannot have saturations less than zero or greater than 100% is extremely valuable prior information and becomes increasingly pertinent as the saturation approaches the boundary.

Fig. 7 describes the variation of P- and S-wave impedances and attenuation ($1/Q$) with respect to S_{CO_2} and frequency. This figure explains some of the features in the information curves. For example, low values of $1/Q_P$ at the highest values of S_{CO_2} (Fig. 7c)

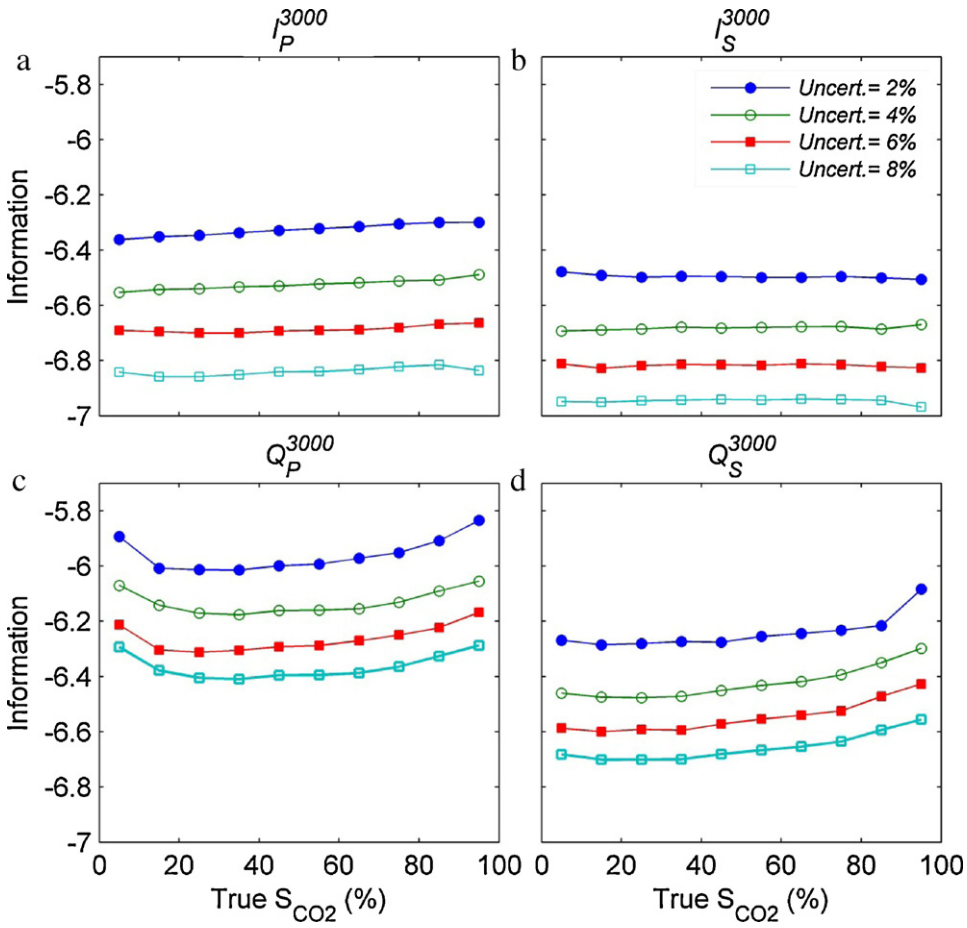

Fig. 5. Information values for different geophysical parameters as a function of true S_{CO_2} inverted from (a) P-wave impedance I_P, (b) S-wave impedance I_S, (c) P-wave quality factor (reciprocal of attenuation) Q_P and (d) S-wave quality factor Q_S estimates each with four different uncertainties, 2%, 4%, 6% and 8% at f = 3000 Hz. The prior pdfs for S_{CO_2}, porosity and clay content are uniform in ranges 0–100%, 0–40% and 0–50%, respectively.

coincide with the low values of $I\left(Q_P^{30}\right)$ in Fig. 4. Insensitivity of $1/Q_P$ to high values of S_{CO_2} has dominated over the hard boundary condition effect in that case. Insensitivity of $I\left(I_S^{30}\right)$, $I\left(I_S^{3000}\right)$ and $I\left(Q_S^{30}\right)$ to S_{CO_2} (Figs. 4 and 5) are also explained by the lack of variation of these parameters with respect to S_{CO_2} and frequency shown in Fig. 7b and d.

4.1. Prior information

Prior information has a prominent impact on the monitorability of the petrophysical changes in the reservoir. If the reservoir is characterized prior to CO_2 injection, reservoir parameters (e.g., porosity) known with some level of uncertainty. Uncertainties in

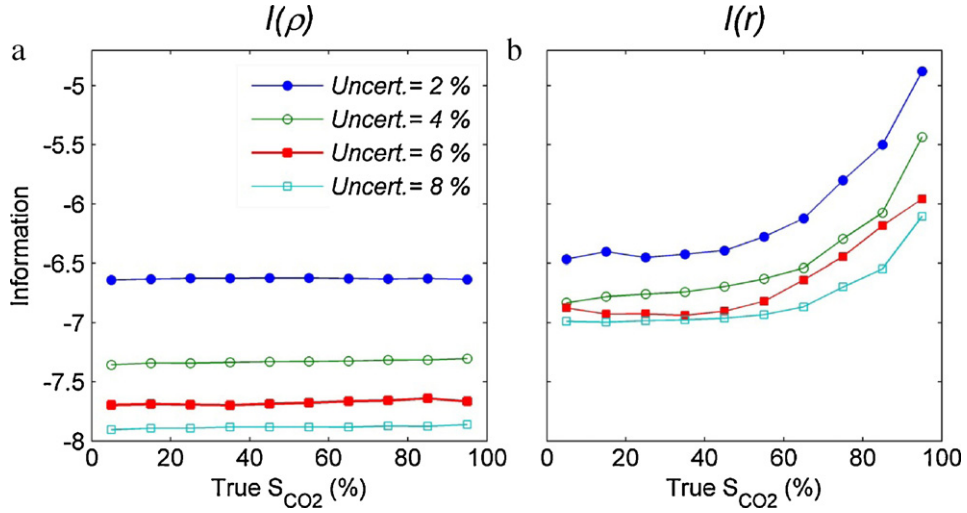

Fig. 6. Information values for different geophysical parameters as a function of S_{CO_2} inverted from (a) resistivity r and (b) density ρ estimates each with four different uncertainties, 2%, 4%, 6% and 8%. The prior pdfs for S_{CO_2}, porosity and clay contents are uniform in ranges 0–100%, 0–40% and 0–50%, respectively.

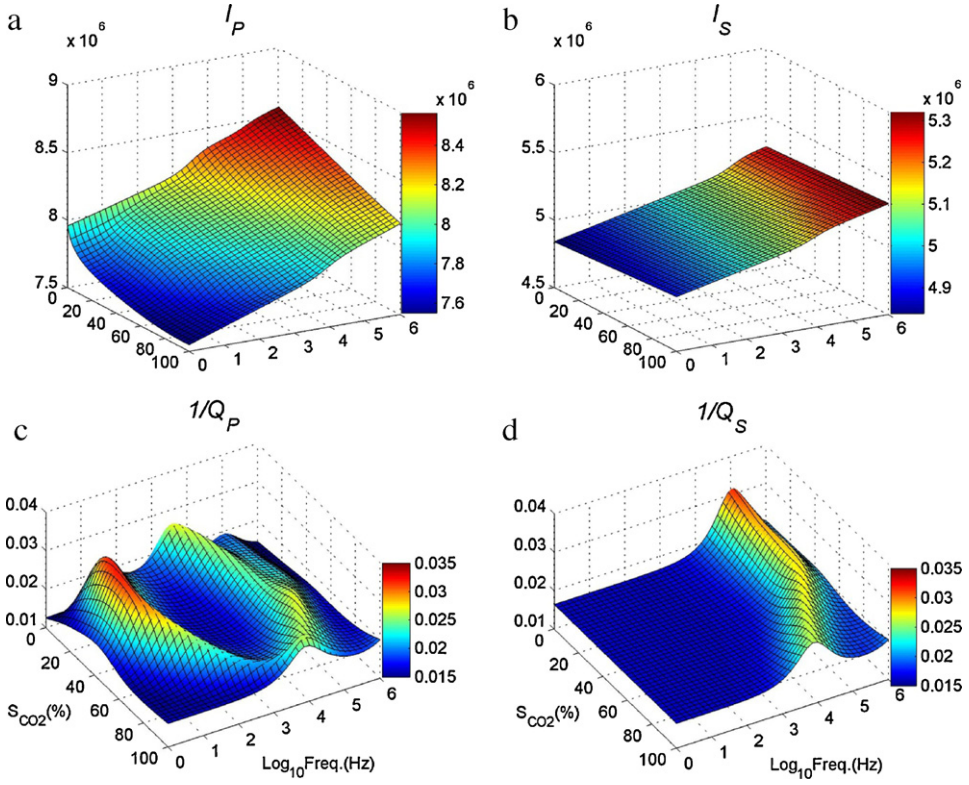

Fig. 7. Variation of the P- and S-wave impedences and attenuations with S_{CO_2} and frequency for the reservoir rock with properties given in Table 1. All horizontal axes are identical and colors reflect the height of each surface. (For interpretation of the references to color in this figure legend, the reader is referred to the web version of the article.)

each one of saturation and porosity have a direct effect on the prediction of the other (e.g., Bachrach, 2006). It is also very likely that the porosity of reservoir rocks varies after injecting CO_2 into brine-saturated aquifers due to both chemical and mechanical effects. Regardless of the cause of the porosity variation, unless accurately estimated, errors will increase the uncertainty in S_{CO_2} estimation. Here we investigate the effect of uncertainty in prior porosity information on the post-inversion information obtained.

Fig. 8a and b depicts calculated average information in the joint pdfs of inverted S_{CO_2} and porosity from different elastic parameters with respect to uncertainties in porosity at $f_1 = 30$ Hz and $f_2 = 3000$ Hz, respectively. Fig. 8c shows calculated average information for ρ and r. The overall information shown is the average of the information calculated for 10 discrete values of true S_{CO_2} from 5% to 95%. We assume uniform prior distributions with different ranges from $\pm 1\%$ to $\pm 11\%$ porosity units of the true porosity (e.g., $22.6 \pm 1\%, 22.6 \pm 2\%, \ldots, 22.6 \pm 11\%$,). We assume uniform prior pdfs for S_{CO_2} and clay content in the ranges 0–100% and 0–50%, respectively, and 2% uncertainty in the geophysical parameter estimates. For comparison, the information of prior joint probability distributions of porosity and S_{CO_2} corresponding to each level of uncertainty is shown with a thick solid line in Fig. 8.

This analysis indicates that generally the information obtained is very sensitive to the prior uncertainties in porosity. However, for higher values of uncertainties in the porosity estimate the sensitivity of $I(Q_P)$ is lower than that of other parameters. $I(r)$ presents the highest sensitivity to the prior uncertainty in porosity. While with low prior uncertainty in porosity $I(r)$ is very high, with uncertainty greater than 9% $I(r)$ is as low as $I(\rho)$ which is the lowest among the six parameters. Fig. 8 implies that more accurate pre-injection reservoir characterization has a large effect on the monitorability of S_{CO_2}. In the case of time-lapse monitoring for example, existing information from the benchmark (pre-injection) survey significantly reduces uncertainties in reservoir parameters.

4.2. Joint application of geophysical parameters

Even though some of the geophysical parameters show promising capabilities in monitoring S_{CO_2} over different ranges of S_{CO_2} and different levels of uncertainty, from a practical point of view there are a range of logistical or economical barriers that affect their efficiency. For example, while electrical resistivity might seem to be an appropriate parameter to be measured in order to monitor S_{CO_2}, very low spatial resolution (including depth resolution) and noise contamination of corresponding field measurement methods such as controlled source electromagnetic (CSEM) reduce the obtained subsurface information. Joint application of multiple geophysical techniques may in some cases simultaneously increase the subsurface information and solve the resolution problem (e.g., Hoversten et al., 2006; Chen et al., 2007).

We now calculate the information of joint pdfs of the inverted S_{CO_2} and porosity from joint inversion of all different pair-wise combinations of geophysical parameters. We assume a reservoir rock with the same properties as used in the previous sections. The prior pdfs for S_{CO_2}, porosity and clay content are uniform in the ranges 0–100%, 0–40% and 0–50%, respectively. Uncertainties in geophysical parameters are 2% and 8% for P- and S-wave impedances and quality factors, respectively, at the low frequency $f_1 = 30$ Hz. At the higher frequency of $f_2 = 3000$ Hz uncertainties in impedances and quality factors are 1% and 4%, respectively, representing the higher accuracy available from well-based measurements. Uncertainty for density and resistivity is 20%. The overall average information that will be shown for each pair is the average of the entropies calculated for 10 discrete values of true S_{CO_2} from 5% to 95%.

Fig. 9 shows the values of average information obtained from joint inversion of the various geophysical parameter pairs. Superscripts 1 and 2 stand for f_1 and f_2 representing surface and well-based measurements, respectively. In this case the highest

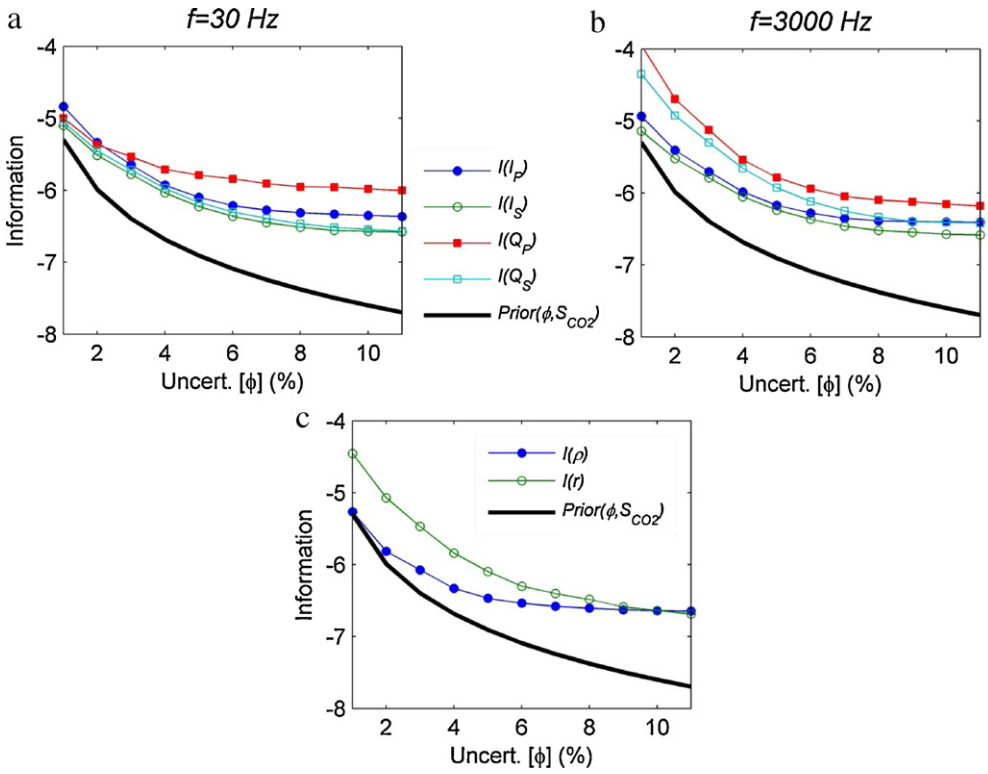

Fig. 8. Variation of information for I_P, I_S, Q_P and Q_S measurements at (a) $f = 30$ Hz, (b) $f = 3000$ Hz and (c) ρ and r, with respect to uncertainty in the porosity values ($\varphi = 22.6\%$) and averaged over 10 discrete and evenly spaced values of S_{CO_2} in a range 5–95%. The prior pdfs for S_{CO_2} and clay content are uniform in ranges 0–100% and 0–50%, respectively. Uncertainty in all of the geophysical parameters is fixed at 2%.

average information is obtained for the joint inversion of I_P^{3000} and Q_P^{30}. However, joint inversion of r with all (an)elastic parameters, as well as Q_P with impedances at both low and high frequencies, also provide high levels of information.

The panel presented in Fig. 9 may be used to design efficient monitoring strategies and can be reproduced for any range of true S_{CO_2}, and any more appropriate volume of geophysical or petrophysical parameter pair uncertainties given a particular field. No

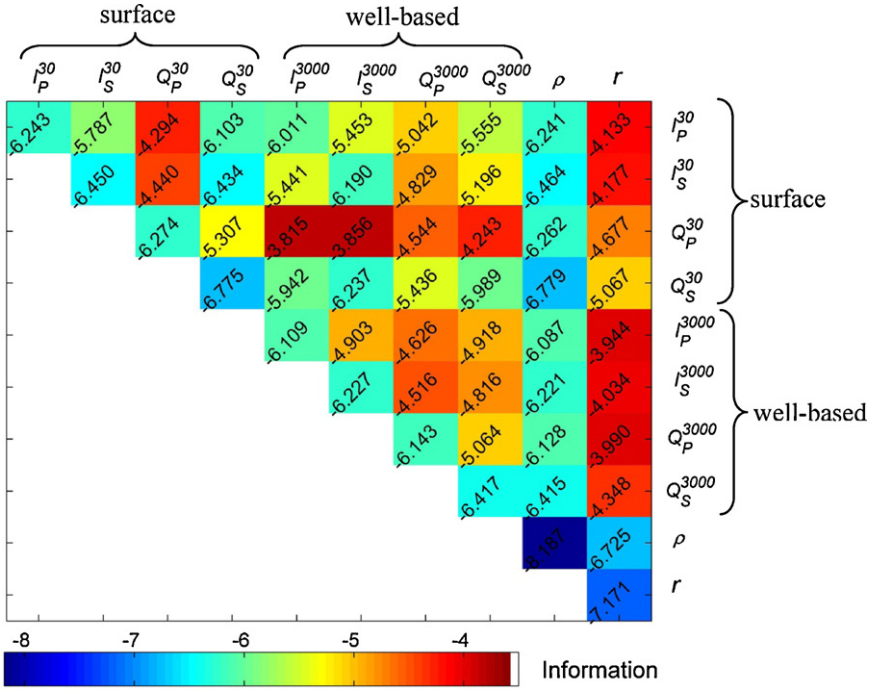

Fig. 9. Average values of information for joint inversion of different geophysical parameters over the range $S_{CO_2} = 0$–100%. The uncertainties in geophysical parameters are 2% and 4% for P- and S-wave impedances and quality factors, respectively, at the low frequency, 1% and 2% for P- and S-wave impedances and quality factors, respectively, at the high frequency, and 20% for density and resistivity. The prior pdfs for S_{CO_2}, porosity and clay contents are uniform in ranges 0–100%, 0–40% and 0–50%, respectively.

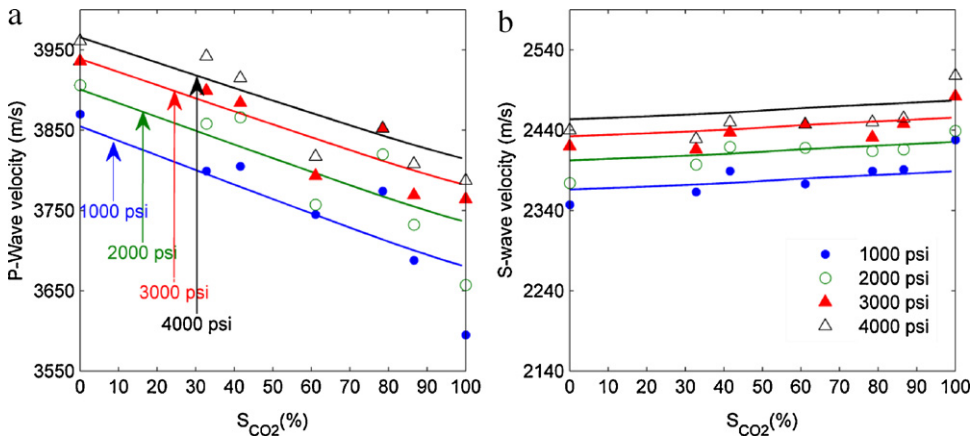

Fig. 10. Variation of measured P-wave (left) and S-wave (right) velocities on sample CL1 at different effective pressures and saturation S_{CO_2}, and the corresponding petrophysical model fit to the measurements (solid lines).

assumption of linearized physics is used to obtain the information values – the full nonlinearity of the petrophysical problem is accounted for. Given expected uncertainties in the geophysical parameters, this panel indicates which geophysical parameters are more appropriate to be used to monitor petrophysical changes in the reservoir.

In this specific case, in addition to joint inversion of well-based estimates of impedances and quality factors, on average the integration of well-based I_P and I_S estimates with the estimated Q_P in surface reflection seismics produces the highest level of information. However, this requires that the area monitored has a sufficient well-based monitoring system to obtain the high frequency I_P and I_S data. Inspection of Fig. 9 shows that on average we forfeit relatively little information by instead monitoring both low frequency I_P and Q_P from the surface. This is an important cost-saving result if it allows fewer wells to be drilled. Although the joint inversion of r and elastic parameters provide high level of information, the low spatial resolution and practical difficulties in estimation make it less likely to be used for monitoring.

5. Monitorability of the CASSEM analogue CO_2 storage site

In this section we assess the monitorability of S_{CO_2} in one of the CASSEM project (CASSEM stands for "CO_2 Aquifer Storage Site Evaluation and Monitoring" – an academic-industrial joint project in the UK) analogue storage sites in the Firth of Forth based on the approach presented in the previous sections. The target aquifer of the Firth of Forth site is in the Kinnesswood and Knox Pulpit Formations in the east of Scotland. The thickness of the reservoir is estimated 300 m. The seal is the Ballagan Formation, and the underlying formation was the Glenvale. The geological interpretation and modelling are described in Ritchie et al. (2003), Underhill et al. (2008) and Monaghan et al. (2009) and uncertainties in the

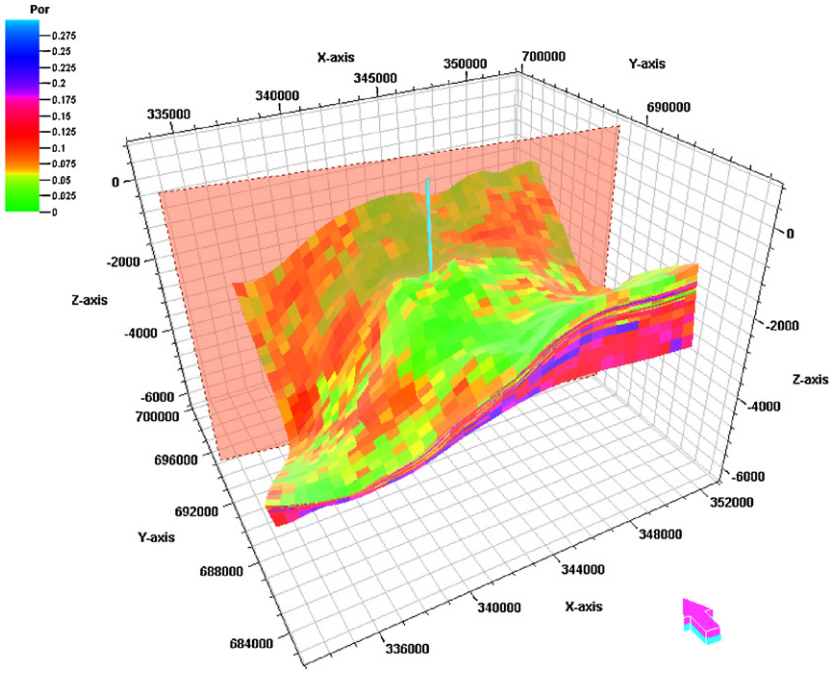

Fig. 11. Spatial configuration of the Firth of Forth aquifer reservoir, the hypothetical injection well, and the selected west–east cross-section through the well. The color scale indicates porosity values and the arrow points to North. (For interpretation of the references to color in this figure legend, the reader is referred to the web version of the article.)

underlying geological reservoir model are investigated in Polson and Curtis (2010).

5.1. Analogue reservoir rock sample

Since no borehole was drilled into the prospecting Firth of Forth analogue reservoir, two rock samples, CL1 and CL2, from Clashach sandstone outcrop in the area (expected to be geologically analogous to the reservoir rock) were used to estimate elastic and electromagnetic properties of the reservoir rocks. Fig. 10 shows the variation of measured P-wave and S-wave velocities with respect to S_{CO_2} at different effective pressures (1000 psi, 2000 psi, 3000 psi and 4000 psi) on sample CL1 with 22.6% porosity. Different saturations are obtained by flooding the sample with supercritical CO_2 and the saturations were calculated based on the volume of water expelled during core flooding. To obtain high S_{CO_2} s, the sample that had been equilibrated in a humidity chamber was saturated with supercritical CO_2. Further details about the laboratory measurements are given in Fisher et al. (2010).

In practice, measurements on a large number of reservoir rock samples should be used to calibrate the petrophysical model before inversion. However, since the main objective of this paper is to develop the methodology, and also due to the limited number of available laboratory measurements on CO_2 saturated samples, we use these data to calibrate the petrophysical model that we use from hereon for Monte Carlo inversion of the geophysical parameters in order to assess monitorability of S_{CO_2} in the Firth of Forth aquifer reservoir. Solid lines in Fig. 10 show the best-fit petrophysical model for each effective pressure. We use the material parameters in Table 1, and 5% clay content for calibration. Note that the best-fit petrophysical model is the same as the model used in the previous sections. The only electromagnetic measurement on sample CL1 is for the brine-saturated sample that indicates its electrical resistivity is 3.5 ohm m. We rely on the above available data and use the combined [White (1975) and Pham et al. (2002)] and Pride (1994) models in Appendix A to describe elastic and electromagnetic parameters, respectively.

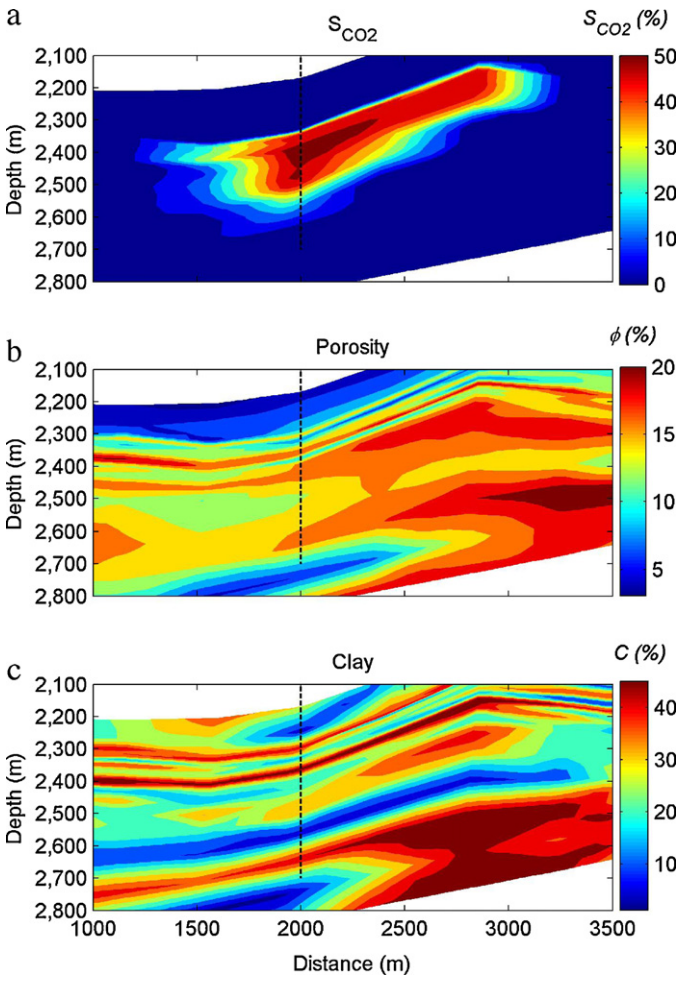

Fig. 12. (a) Spatial distribution of S_{CO_2} after 10 years of injection, (b) porosity and (c) clay content across the west–east cross-section of the Firth of Forth model in Fig. 11.

5.2. Analogue storage site

In the CASSEM project the Firth of Forth site was selected only for the purpose of developing methodology and in practice there will not be any real CO_2 injection. We therefore use the result of a flow simulation to assess the monitorability of the site. Different injection scenarios were examined for the site to predict the distribution of CO_2 in the reservoir after several years of injection. More details about the injection scenario and reservoir are given in Jin et al. (2010). The overall average porosity and permeability of the aquifer are about 0.135 mD and 60 mD, respectively. The petrophysical properties were generated stochastically across the reservoir using PETREL$_{TM}$. We choose a single well injection scenario and study the distribution of CO_2 along an east–west vertical cross-section of the reservoir after 10 years of injection (Fig. 11) to assess the expected monitorability of the Firth of Forth site.

The corresponding spatial distribution of S_{CO_2}, porosity and clay content of the reservoir in the resulting two-dimensional cellular model along the vertical section are shown in Fig. 12. After 10 years of injection the CO_2 plume migrated about 1300 m eastward and 800 m westward along the section. In this scenario it was assumed that there was no leakage into the seal. Effective pressure in the reservoir varies from 25 MPa at the top to about 32 MPa at the bottom of the reservoir around the injection well.

Evaluation of uncertainty associated with the spatial distribution of free CO_2 in the reservoir is an objective of geophysical monitoring that might significantly contribute to reducing the perception of risk of leakage. We assume that time-lapse reflection seismics and CSEM surveys have been deployed over the reservoir. We produce synthetic sections of geophysical parameters along the reservoir interval based on the flow simulation results. We follow the workflow in Fig. 3 and invert simulated geophysical parameters to estimate S_{CO_2} in the reservoir as in the previous sections.

CSEM data typically results in far lower spatial resolution than reflection seismic data. To represent the different resolutions we treated CSEM data as highly spatially averaged data as would be obtained in a real survey. To mimic this approximately we therefore applied a smoothing filter to the cross-section of porosity and saturation values by averaging them over many surrounding model cells. Then, for each cell we use the petrophysical model to calculate resistivity from the averaged porosity and saturation. We use the above Monte Carlo approach for inversion. We assume the prior pdfs for S_{CO_2}, porosity and clay content are uniform in the ranges 0–100%, 0–40% and 0–50%, respectively. We also assume that the errors in estimated geophysical parameters are Gaussian and assign 2%, 8% and 20% standard deviation (STD) to the impedances, quality factors and resistivity estimates, respectively, corresponding to the seismics and CSEM methods. Density can be estimated either from seismics or from gravity measurements, however, the spatial resolution would be significantly different. In this case, we assume that density is estimated from seismics with 20% uncertainty.

We calculate the information of the joint marginal posterior distribution of S_{CO_2} and porosity in each model cell for different combination of geophysical measurements. Fig. 13a–f show spatial

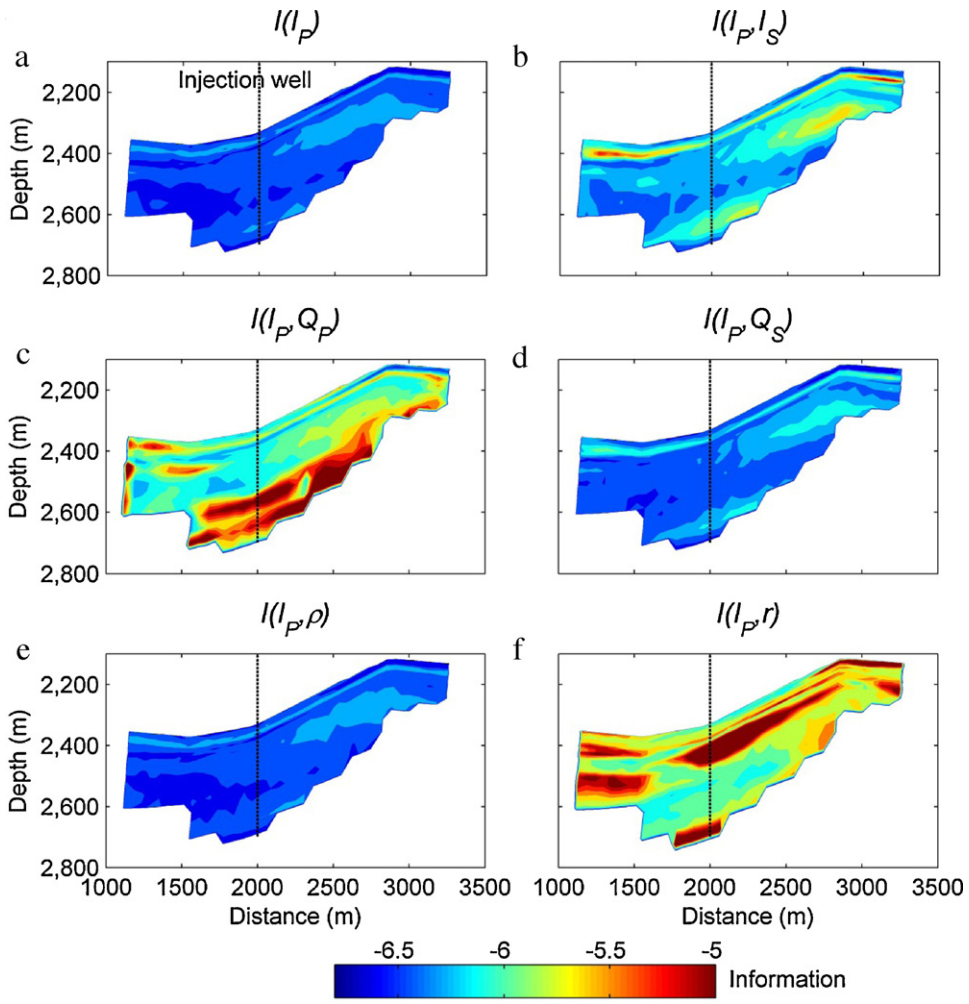

Fig. 13. (a) Distribution of calculated information of joint posterior distributions of S_{CO_2} and porosity from inversion of I_P, (b) from joint inversion of I_P and I_S, (c) from joint inversion of I_P and Q_P, (d) from joint inversion of I_P and Q_S, (e) from joint inversion of I_P and ρ, and (f) from joint inversion of I_P and r across the west–east cross-section of the Firth of Forth model in Fig. 13. Frequency of seismic measurements is 30 Hz. The prior pdfs and uncertainties in geophysical parameters are the same as those for Fig. 9.

variation in $I(I_P)$ and five different pair-wise combinations of geophysical parameters, $I(I_P,I_S)$, $I(I_P,Q_P)$, $I(I_P,Q_S)$, $I(I_P,\rho)$ and $I(I_P,r)$, over the reservoir cross-section. The results shown in Fig. 13 are in agreement with the design panel (Fig. 9) where joint inversion of geophysical parameters significantly increases the information obtained, and hence improves our monitoring capabilities by decreasing the uncertainties associated with saturation prediction. Spatial distribution of $I(I_P)$ indicates a number of low information zones along the vertical cross-section. Each of five pair-wise combinations of geophysical parameters used for joint inversion improves the uncertainty in these zones with different degrees of efficiency. In particular, joint inversion of the I_P and Q_P pair is the most effective at reducing the uncertainties. Although estimation of Q_P requires elaborate processing, the fact that it can be extracted from the same data set as I_P (in contrast to resistivity estimates that require separate field instrumentation) makes it an appropriate parameter to be estimated, particularly from a low-cost monitoring point of view.

Identifying the spatial distribution of low information zones is extremely valuable for designing surveys and ultimately for risk mitigation as they represent "shadow" zones into which we have little geophysical viability. In order to interpret the spatial distribution of information (Fig. 13) were late the information obtained along the vertical cross-section to the product of the true values of porosity, clay content and S_{CO_2} (Fig. 12) in the reservoir which is a dimensionless parameter analogous to the CO_2 volume,

$$PV_{CO_2} = \phi S_{CO_2}(1 - Cly), \tag{7}$$

where ϕ and Cly indicate porosity and clay content, respectively. Fig. 14a–d shows the joint pdf's (normalised histograms) of PV_{CO_2} calculated from the true reservoir parameters (Fig. 12) and estimated information $I(I_P)$, $I(I_P,I_S)$, $I(I_P,Q_P)$ and $I(I_P,r)$, respectively, at all model cells along the reservoir cross-section. Fig. 14a indicates that in general the information obtained at the model cells with high concentration of CO_2 are slightly higher than the information obtained at the model cells with low concentration of CO_2. As can be seen in Fig. 14c, joint inversion of I_P and Q_P provides additional information at low and intermediate CO_2 concentrations which is due to mesoscopic-scale fluid induced attenuation at intermediate S_{CO_2}. Joint inversion of I_P and r provides significant information at high CO_2 concentrations, and joint inversion of I_P and I_S evenly increases the information at all CO_2 concentrations.

6. Discussion

Evaluating the information expected from different combinations of measurable geophysical parameters is useful in order to justify surveying and processing costs of the corresponding

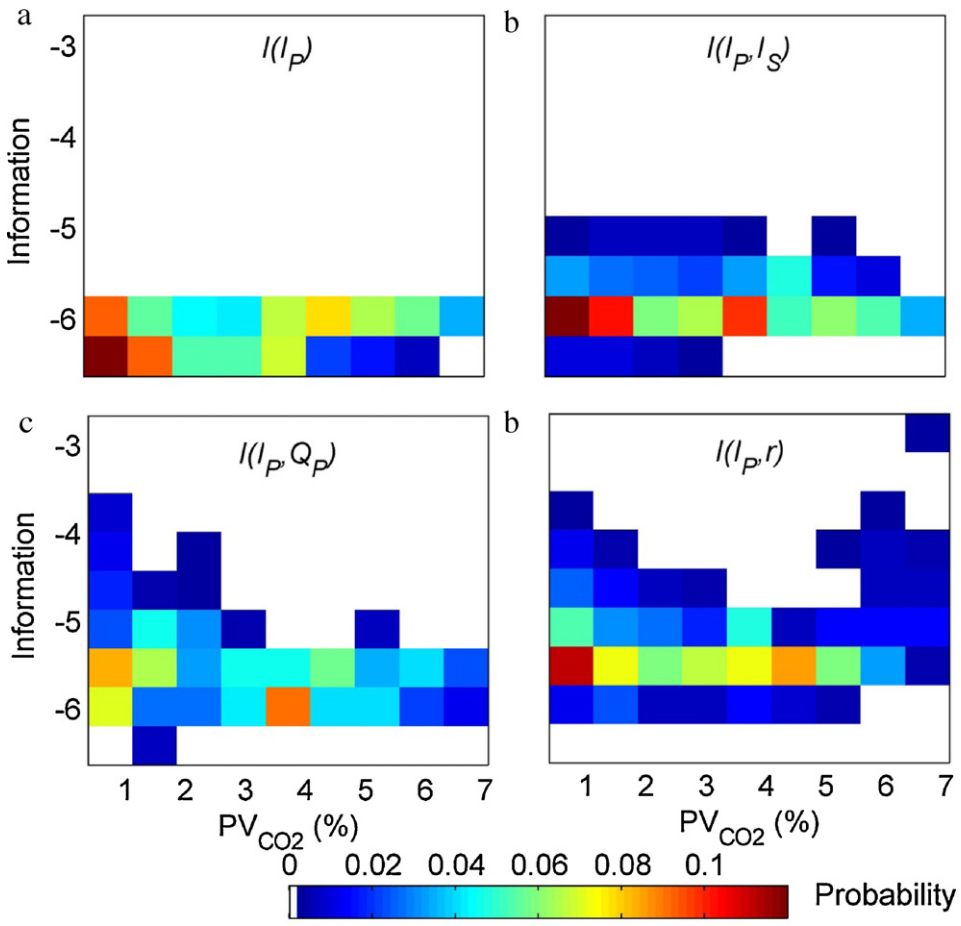

Fig. 14. (a) Probability distribution of PV_{CO_2} and information obtained from inversion of I_P, (b) from joint inversion of I_P and I_S, (c) from joint inversion of I_P and Q_P, and (d) from joint inversion of I_P and r.

data. Knowledge about the expected information becomes valuable when the long-term benefits of a monitoring plan, and its expected contribution to risk mitigation, are included in the field development strategy. Identification of shadow zones within which there is diminished geophysical visibility may be critical, particularly in a CO_2 storage scenario if the shadow zones are in the cap-rock or overburden meaning that leaks into such zones may not be detected. Even if the result of the workflow herein is negative in the sense that a site cannot be adequately monitored, this knowledge reduces field development risk: a field that cannot be verified as a safe and secure store is not a viable CCS prospect – the field can be abandoned without further wasted investment.

In this paper we used six geophysical parameters (I_P, I_S, Q_P, Q_S, ρ, and r) that represent the results from some of the most commonly used geophysical methods. There are a range of other monitoring techniques such as satellite measurements of Earth surface movements and microseismic monitoring that are related to the geomechanical behaviour of the rocks. Even though they have proved to be efficient in monitoring some subsurface reservoirs in the past (e.g., Onuma and Ohkawa, 2009; Verdon et al., 2010; Maxwell et al., 2010; Rucci et al., 2010), to keep the scope of our work reasonable we do not investigate them in this paper. Nevertheless, there is no reason why the same methodology as herein, and as shown in Fig. 3, will not work for such data in future.

Figs. 4 and 7 indicate that when the effect of mesoscopic-scale fluid induced seismic attenuation is also measured there is a considerable improvement over the information obtained from the inversion of elastic parameters. Within White's (1975) model this effect is represented by the size of the fluid patches. In the examples presented in the previous sections we assumed patches of equal size. This was arbitrary, and a representative value of patch size may be different in different reservoirs. Generally, the injection of supercritical CO_2 into brine-saturated reservoirs is expected to lead to patchiness in the saturation, however the fluid patchiness may vary with time, distance from the injection point and with reservoir rock characteristics. For example, Xue and Lei (2006) deployed P-wave velocity tomography on the velocity data recorded using an array of piezoelectric transducers mounted on a core sample. Their imaging results show a spatially heterogeneous distribution of P-wave velocity in partially saturated conditions. Later, Shi et al. (2007) analysed the same data and concluded that the considerable variation in the P-wave velocity across the sample could largely be attributed to the state of saturation (uniform, patchy, or between these two end-member states) in different sections of the sample. Based on the same dataset, Lei and Xue (2009) indicate that in the realistic CO_2 saturation ranges ($S_{CO_2} < \sim 50\%$), P-wave attenuation is very sensitive to CO_2 saturation, which confirms the significant impact of the patchy saturation pattern. Considering spatial and temporal variation of the partial saturation characteristic in the inversion may improve the subsurface information obtained. However, application of such laboratory-scale research to field-scale problems is not straightforward, and the nonlinear effect of frequency as well as large-scale reservoir heterogeneities (e.g., faults) and injection rate must be taken into account. Since this paper is more focused on the development of methods to assess different possible survey data types, we leave further investigation of the spatial and temporal variation of the saturation type across the reservoir for future work.

7. Conclusion

We propose an approach to assess the geophysical monitorability of subsurface reservoirs and to predict the expected uncertainty in the distribution of saturation. We developed the approach within the framework of assessing the monitorability of supercritical CO_2 saturation S_{CO_2} where CO_2 is to be stored in saline aquifer reservoirs. We assess the effects of uncertainties in geophysical and petrophysical parameters on the monitorability of S_{CO_2}. Application of the approach to hydrocarbon saturation estimation and monitoring is straightforward.

The approach is based on the Monte Carlo inversion of six geophysical parameters: P- and S-wave impedances I_P and I_S and quality factors Q_P and Q_S, density ρ, and electrical resistivity r. To design an appropriate monitoring strategy, we assess the amount of information that each of the six geophysical parameters would be likely to provide about key reservoir parameters (e.g., S_{CO_2}), both individually and in combination with each other. In order to quantify the obtained information from the inversion of different geophysical parameters we use Shannon's information measure which is a single valued measure of the information described by a probability density function (pdf). Results show that the information expected to be obtained is nonlinearly related to the level of uncertainty in the geophysical and petrophysical parameters, and in the case of seismic measurements also to the measurement frequency. Prior uncertainties in petrophysical parameters such as porosity have a considerable impact on the monitorability of S_{CO_2}, which highlights the importance of accurate information from benchmark (pre-injection) measurements and of reservoir characterization in the case of time-lapse monitoring.

We show that seismic attenuation contributes greatly to the overall information obtained, due to the mesoscopic-scale interaction between seismic waves and fluids in the reservoir. We also show that a combination of different geophysical parameters and methods (e.g., seismics and electromagnetics – EM) can significantly increase the overall information obtained and improve monitorability and quantification of S_{CO_2} in aquifer reservoirs. This could be achieved by designing an optimal combination of borehole and surface measurements of different types, using the information-based methods herein. Borehole measurements increase petrophysical resolution, while surface measurements provide the required geophysical spatial resolution for monitoring over reservoirs of large lateral extent.

We applied the proposed approach to assess monitorability of S_{CO_2} after 10 years of hypothetical (modelled) CO_2 injection in a saline aquifer reservoir in the UK North Sea and estimate the spatial distribution of information along a vertical cross-section of the reservoir. Results show that while the inversion of estimated I_P from surface reflection seismics may not provide a high level of information about the reservoir parameters, the information obtained from joint inversion of I_P and Q_P is significantly greater. EM measurements only have the potential to aid reservoir monitoring, provided they can provide adequate spatial resolution of subsurface resistivity.

Acknowledgments

The research related to this paper has been carried out within the CASSEM project, which is a project supported by the Technology Strategy Board. The authors wish to acknowledge the support of, the TSB and the EPSRC and the project industry partners; AMEC, Marathon, Schlumberger, Scottish Power, and Scottish and Southern Energy, and the academic partners; British Geological Survey, Heriot-Watt University, University of Edinburgh, and the University of Manchester. We thank Quentin Fisher and his colleagues at the University of Leeds for providing us with the laboratory measurements on the CO_2 saturated samples.

Appendix A. Petrophysical model

Pham et al. (2002) developed their petrophysical model based on the theory developed by Carcione et al. (2000) that takes into account the presence of three phases: sand grains, clay particles and fluid. Carcione et al. (2000) solved the equation of motion to derive velocities and attenuation. The three compressional and shear velocities and attenuation of the three-phase porous media are given by

$$V_{ij} = \left[Re\left(\sqrt{\chi_{ij}}\right)\right]^{-1}, \tag{A-1}$$

and

$$Q_{ij} = -\frac{Re(V_{ij})}{Im(V_{ij})}, \tag{A-2}$$

where $j = 1$, 2 and 3 denote sand, water and clay respectively, $i = 1$ and 2 indicate P and S waves respectively, Re and Im denote real and imaginary parts respectively, and χ_{ij} are obtained from the generalized characteristic equations $\det\left(\chi_{1j}\mathbf{R} - \tilde{\rho}\right) = 0$ and $\det\left(\chi_{2j}\boldsymbol{\mu} - \tilde{\rho}\right) = 0$, for P and S waves, respectively. The characteristic equations are obtained from the matrix form of the equation of motion.

$$\mathbf{R}\Delta\nabla\mathbf{u} - \boldsymbol{\mu}\nabla\times\nabla\times\mathbf{u} = \boldsymbol{\rho}\ddot{\mathbf{u}} + \mathbf{B}\dot{\mathbf{u}}, \tag{A-3}$$

where $\mathbf{u}$ is the displacement field,

$$\mathbf{R} = \begin{bmatrix} R_{11} & R_{12} & R_{13} \\ R_{12} & R_{22} & R_{23} \\ R_{13} & R_{23} & R_{33} \end{bmatrix} \text{ and } \boldsymbol{\mu} = \begin{bmatrix} \mu_{11} & 0 & \mu_{13} \\ 0 & 0 & 0 \\ \mu_{13} & 0 & \mu_{33} \end{bmatrix}$$

are the bulk and shear stiffness matrices, respectively,

$$\boldsymbol{\rho} = \begin{bmatrix} \rho_{11} & \rho_{12} & \rho_{13} \\ \rho_{12} & \rho_{22} & \rho_{23} \\ \rho_{13} & \rho_{23} & \rho_{33} \end{bmatrix} \text{ and } \mathbf{B} = \begin{bmatrix} B_{11} & B_{12} & 0 \\ B_{12} & B_{22} & B_{23} \\ 0 & B_{23} & B_{33} \end{bmatrix}$$

are mass density and the friction matrices, respectively. The detailed expressions of the different coefficients as a function of the properties of constituents are given by Carcione et al. (2000). The bulk and shear moduli of the sand and clay matrices at a specific depth are given by

$$K_{jm} = K_j \frac{S_j}{(1-\phi)}(1-\phi)^{(1+A)/(1-\phi)}, \tag{A-4}$$

$$\mu_{jm} = \frac{K_{jm}\mu_j}{K_j}, \tag{A-5}$$

where $j = 1$ and 3 for sand and clay, respectively, K_j and μ_j are bulk and shear moduli of particles, and the S_j indicate sand and clay contents ($S_1 + S_3 + \phi = 1$). The pressure dependency of the rock modulus is contained in Eq. (A-4) through parameter A. Pham et al. (2002) assumed the dependency of the dry rock moduli to the effective pressure at a specific depth is

$$K_{1m} = \beta K_{HS}\left\{1 - \exp\left[\frac{p_e(p)}{p_K^*}\right]\right\}, \tag{A-6}$$

$$\mu_{1m} = \beta \mu_{HS}\left\{1 - \exp\left[\frac{p_e(p)}{p_\mu^*}\right]\right\}, \tag{A-7}$$

where p^* is obtained by fitting Krief et al. (1990) expression (A-7), p_e is effective pressure and K_{HS} and μ_{HS} are Hashin–Shtrikman (HS) upper bunds (Hashin and Shtrikman, 1963). To incorporate partial

saturation, Pham et al. (2002) introduced the effective fluid bulk modulus by an empirical mixing law

$$K_f = \left(K_w - K_g\right) S_w^e + K_g, \tag{A-8}$$

(Brie et al., 1995) where $e = \left(f/f_0\right)^{0.34}$ with f_0 being a reference frequency that indicates upper frequency limit of the model validity. Setting $e = 1$ in equation (A-8) gives Voigt's fluid mixing law, which we use in this paper. In equation (A-8) since the partial saturation model requires partial permeabilities, a generalized form of Kozeny–Carmen relationship (Dullien, 1991) is used as

$$\kappa = B\left(\phi - \phi_p\right)^3 d^2 T^{-1} \left[\kappa_{rw} S_w + \kappa_{rg}\left(1 - S_w\right)\right], \tag{A-9}$$

where B is a geometrical factor, d is effective grain size, T is the tortuosity of the mixture, ϕ_P is percolation porosity (e.g., Mavko and Nur, 1997), κ_{rw} and κ_{rg} are normalised permeabilities given by

$$\kappa_{rw} = \sqrt{S_{we}}\left[1 - \left(1 - S_{we}^{1/m_w}\right)^{m_w}\right]^2,\ S_{we} = \frac{S_w - S_{wi}}{1 - S_{wi}}, \tag{A-10}$$

$$\kappa_{rg} = \sqrt{S_{ge}}\left[1 - \left(1 - S_{ge}^{1/m_g}\right)^{m_g}\right]^2,\ S_{ge} = \frac{S_g - S_{gi}}{1 - S_{gi}}, \tag{A-11}$$

where S_{wi} and S_{gi} are irreducible water saturation and trapped gas, respectively. Pham et al. (2002) introduced viscoelastic attenuation into their model by making the bulk and shear moduli of the sandstone skeleton viscoelastic. They modified these moduli by the constant-Q kernel

$$M(\omega, Q) = \left(\frac{i\omega}{\omega_0}\right)^{2\gamma},\ \ \gamma = \frac{1}{\pi}\tan^{-1}\left(\frac{1}{Q}\right), \tag{A-12}$$

where $\omega_0 = 2\pi f_0$.

The high frequency viscodynamic effects are employed by substituting

$$b_{jj} = \left(\frac{\mu_f \phi^2}{\kappa_j}\right) F_j(\omega),\ j = 1, 3 \tag{A-13}$$

where F_j represents viscodynamic function correspond to the interaction between sand and clay matrices with the fluid (e.g., Biot, 1962; Johnson et al., 1987).

A.1. White's model of a layered porous media

White (1975) obtained the complex bulk modulus for a P-wave travelling perpendicular to the stratification in a layered media composed of two porous media with thicknesses d_l, $l = 1, 2$, and saturations of $S_l = [d_l/(d_1 + d_2)]$. Following the Carcione and Picotti (2006) and Picotti et al. (2010) rearrangements of White's equations the White's bulk modulus is given by

$$E(\omega) = \left\{\frac{1}{E_\infty} + \frac{2\left[\alpha\left(M_1/K_{G1} - M_2/K_{G2}\right)\right]^2}{[i\omega(d_1 + d_2)(I_1 + I_2)]}\right\}^{-1}, \tag{A-14}$$

where

$$E_\infty = \left(\frac{S_1}{K_{G1}} + \frac{S_2}{K_{G1}}\right)^{-1}, \tag{A-15}$$

and K_{G1} and K_{G2} are Gassmann bulk moduli Gassmann (1951) given by

$$K_{Gl} = K_{1m} + \alpha^2 M_l,\ M_l = \left(\frac{\alpha - \phi}{K_1} + \frac{\phi}{K_{fl}}\right)^{-1},\ \alpha = 1 - \frac{K_{1m}}{K_1}, \tag{A-16}$$

and

$$I_l = \frac{\eta_l}{\kappa k_l}\coth\left(\frac{k_l d_l}{2}\right), \tag{A-17}$$

where η_l is fluid viscosity, k_l is the complex wavenumber of the slow P-wave velocity given by

$$k_l = \sqrt{\frac{i\omega\eta_l K_{Gl}}{\kappa M_l\left(K_{1m} + \frac{4}{3}\mu_{1m}\right)}} \tag{A-18}$$

A.2. Combined model

In order to obtain a comprehensive model that is able to represent mesoscopic-scale fluid effects on the seismic waves in addition to microscopic and viscoelastic effects, we combine White's model of layered porous media with the model of Pham et al. (2002). To do so, we extract the frequency dependency of the complex bulk modulus of White's model (equation (A-14)),

$$\xi(\omega) = \frac{E(\omega) - 4/3\mu_{1m}}{K_{1m} + \alpha^2 M_f}, \tag{A-19}$$

where

$$M_f = \left(\frac{\alpha - \phi}{K_1} + \frac{\phi}{K_f}\right)^{-1}, \tag{A-20}$$

and modify the sand skeleton bulk modulus in equation (A-6)

$$K_{1m} \to K_{1m}\xi(\omega) \tag{A-21}$$

A.3. Pride's (1994) model for electrical resistivity

The electrical conductivity (1/resistivity) of porous rocks as a function of salinity of pore fluid and permeability, is obtained by using Pride's (1994) model as

$$\tilde{\sigma} = \left(\frac{\phi\sigma_f}{\chi}\right)\left[1 + \frac{2\left[C_{em} + Re\left(C_{os}(\omega)\right)\right]}{\sigma_f \Lambda}\right], \tag{A-22}$$

where ω is the angular frequency, ϕ is the porosity, σ_f is the fluid conductivity, χ is tortuosity and

$$\Lambda = \sqrt{\frac{\xi\chi\kappa}{\phi}} \tag{A-23}$$

is a geometrical parameter related to the surface-to-pore volume ratio with κ being permeability and $\xi = 8$ for a set of non-intersecting canted tubes. C_{em} is the excess conductance associated with the electromigration of double-layer ions, and C_{os} is the electro-osmotic conductance (for more details about parameters of equation (A-22), see Carcione et al., 2003). We introduce the tortuosity as

$$\chi = \left[\frac{1}{\chi_s}\left(1 - \frac{S_c}{S_c + S_s}\right) + \frac{1}{\chi_c}\left(\frac{S_c}{S_c + S_s}\right)\right]^{-1} \tag{A-24}$$

where $\chi_s = 1 + S_s/2\phi$ and $\chi_c = 1 + S_c/2\phi$ are sand and clay tortuosities and S_s and S_c are sand and clay contents, respectively (Carcione et al., 2000). The permeability is described by the Kozeny–Carman relationship (Dullien, 1991),

$$\kappa = G\phi^3 \bar{d}^2 \chi^{-1}, \tag{A-25}$$

where G is an empirical geometrical factor that Pham et al. (2002) set equal to 15, and $\bar{d}$ is the effective grain size defined by,

$$\bar{d} = \left[\frac{1}{d_s}\left(1 - \frac{S_c}{S_c + S_s}\right) + \frac{1}{d_c}\left(\frac{S_c}{S_c + S_s}\right)\right]^{-1}, \tag{A-26}$$

where d_s and d_c are the grain diameter of the sand and clay particles, respectively.

References

Ahmed, N.A., Gokhale, D.V., 1989. Entropy expressions and their estimators for multivariate distributions. Information theory. IEEE Transactions 35, 688–692.

Ajo-Franklin, J., 2009. Optimal experiment design for time-lapse traveltime tomography. Geophysics 74, Q27–Q40.

Alnes, H., Eiken, O., Stenvold, T., 2008. Monitoring gas production and CO_2 injection at Sleipner field using time-lapse gravimetry. Geophysics 73, WA155–WA161.

Archie, G.E., 1942. The electrical resistivity log as an aid in determining some reservoir characteristics. Transaction of American Institute of Mining, Metallurgical and Petroleum Engineers 146, 54–62.

Arts, R., Eiken, O., Chadwick, A., Zwegel, P., van der Meer, B., Zinszner, B., 2004. Monitoring of CO_2 injection at Sleipner using time-lapse seismic data. Energy 29, 1383–1392.

Bachrach, R., 2006. Joint estimation of porosity and saturation using stochastic rock-physics modelling. Geophysics 71, O53–O63.

Biot, M.A., 1956. Theory of propagation of elastic waves in a fluidsaturated porous solid, I: low-frequency range. Journal of the Acoustic Society of America 28, 168–178.

Biot, M.A., 1962. Mechanics of deformation and acoustic propagation in porous media. Journal of Applied Physics 33, 1482–1498.

Bosch, M., Cara, L., Rodrigues, J., Navarro, A., Diaz, M., 2007. A Monte Carlo approach to the joint estimation of reservoir and elastic parameters from seismic amplitudes. Geophysics 72, O29–O39.

Brie, A., Pampur, F., Marsala, A.F., Meazza, O., 1995. Shear sonic interpretation in gas-bearing sands. In: SPE Annual Technical Conference No. 30595, pp. 701–710.

Carcione, J.M., Gurevich, B., Cavallini, F., 2000. A generalized Biot–Gassmann model for the acoustic properties of shaley sandstones. Geophysical Prospecting 48, 539–557.

Carcione, J.M., Seriani, G., Gei, D., 2003. Acoustic and electromagnetic properties of soils saturated with salt water and NAPL. Journal of Applied Geophysics 52, 177–191.

Carcione, J.M., Picotti, S., 2006. P-wave seismic attenuation by slow-wave diffusion: effects of inhomogeneous rock properties. Geophysics 71, O1–O8.

Chen, J., Dickens, T.A., 2009. Effect of uncertainty in rock-physics models on reservoir parameters estimation using seismic amplitude variation with angle and controlled-source electromagnetics data. Geophysical Prospecting 57, 61–74.

Chen, J., Hoversten, G.M., Vasco, D., Rubin, Y., Hou, Z., 2007. A Bayesian model for gas saturation estimation using marine seismic AVA and CSEM data. Geophysics 72, WA85–WA95.

Coles, D., Curtis, A., 2010. Efficient nonlinear Bayesian survey design by DN-optimization. Geophysics 76, Q1–Q8, doi:10.1190/1.3552645.

Cover, T.M., Thomas, J.A., 2006. Elements of Information Theory. Wiley.

Curtis, A., 1999a. Optimal experiment design: cross-borehole tomographic examples. Geophysical Journal International 136, 637–650.

Curtis, A., 1999b. Optimal design of focussed experiments and surveys. Geophysical Journal International 139, 205–215.

Curtis, A., 2004a. Theory of model-based geophysical survey and experimental design. Part A: linear problems. The Leading Edge 23, 997–1004.

Curtis, A., 2004b. Theory of model-based geophysical survey and experimental design. Part B: nonlinear problems. The Leading Edge 23, 1112–1117.

Curtis, A., Michelini, A., Leslie, D., Lomax, A., 2004. Deterministic design of geophysical surveys by linear-dependence reduction. Geophysical Journal International 157, 595–606.

Daley, T.M., Myer, L.R., Peterson, J.E., Majer, E.L., Hoversten, G.M., 2008. Time-lapse crosswell seismic and VSP monitoring of injected CO_2 in a brine aquifer. Environmental Geology 54, 1657–1665.

Dullien, F.A.L., 1991. One and two phase flow in porous media and pore structure. In: Bideau, D., Dodds, J. (Eds.), Physics of Granular Media. Science Publishers Inc, New York, pp. 173–214.

Dutta, N.C., Seriff, A.J., 1979. On White's model of attenuation in rocks with partial gas saturation. Geophysics 44, 1806–1812.

Fisher, Q.J., Martin, J., Grattoni, C., Angus, D., Guise, P., 2010. Ultrasonic velocity and electromagnetic property analysis of sandstone samples with varying brine and supercritical CO_2 saturations. British Geological Survey, CASSEM project report.

Gasperikova, E., Hoversten, M., 2008. Gravity monitoring of CO_2 movement during sequestration: model studies. Geophysics 73, WA105–WA112.

Gassmann, F., 1951. Über die Elastizität poröser Medien. Vierteljahrsschrift der Naturforschenden Gesellschaft in Zürich 96, 1–23.

Guest, T., Curtis, A., 2009. Iteratively constructive sequential design of experiments and surveys with nonlinear parameter-data relationships. Journal of Geophysical Researches 114, B04307, doi:10.1029/2008JB005948.

Guest, T., Curtis, A., 2010. Optimal trace selection for amplitude-variation-with-angle_AVA_ processing of shale-sand reservoirs. Geophysics 75, C37–C47.

Guest, T., Curtis, A., 2011. On standard and optimal designs of industrial-scale 2D seismic surveys. Geophysical Journal International 186, 825–836.

Hashin, Z., Shtrikman, S., 1963. A variational approach to the theory of the elastic behaviour of multiphase materials. Journal of Mechanical & Physical Solution 11, 127–140.

Haszeldine, S., 2009. Carbon capture and storage: how green can black be? Science 325, 1647–1651.

Hoversten, G.M., Cassassuce, F., Gasperikova, E., Newman, G.A., Chen, J., Rubin, Y., Hou, Z., Vasco, D., 2006. Direct reservoir parameter estimation using joint inversion of marine seismic AVA and CSEM data. Geophysics 71, C1–C13.

Huber, M.F., Bailey, T., Durrant-Whyte, H., Hanebeck, U.D., 2008. On entropy approximation for gaussian mixture random vectors, in Multisensor Fusion and Integration for Intelligent Systems, MFI. In: IEEE International Conference, pp. 181–188.

JafarGandomi, A., Curtis, A., 2010. Assessing monitorability of CO_2 saturation in subsurface aquifers. SEG Expanded Abstracts 29, 2703–2708.

Jin, M., Pickup, J., Mackay, E., Todd, A., Monaghan, A., Naylor, M., 2010. Static and Dynamic Estimates of CO_2 Storage Capacity in Two Saline Formations in the UK. SPE131609.

Johnson, D.L., Koplik, J., Dashen, R., 1987. Theory of dynamic permeability and tortuosity in fluid-saturated porous media. Journal of Fluid Mechanics 176, 379–402.

Krause, A., Singh, A., Guestrin, C., 2008. Near-optimal sensor placements in Gaussian processes: theory, efficient algorithm and empirical studies. Journal of Machine Learning Research 9, 235–284.

Krief, M., Garat, J., Stellingwerff, J., Ventre, J., 1990. A petrophysical interpretation using the velocities of P and S waves (full waveform sonic). The Log Analyst 31, 355–369.

Larsen, A.L., Ulvmoen, M., Omre, H., Buland, A., 2006. Bayesian lithology/fluid prediction and simulation on the basis of a Markov-chain prior model. Geophysics 71, R69–R78.

Lei, X., Xue, Z., 2009. Ultrasonic velocity and attenuation during CO_2 injection into water-saturated porous sandstone: measurements using difference seismic tomography. Physics of the Earth and Planetary Interiors 176, 224–234.

Lindley, D., 1956. On a measure of the information provided by an experiment. Annals of Mathematical Statistics 27, 986–1005.

Lomax, A., Michelini, A., Curtis, A., 2009. Earthquake location, direct, global-search methods. In: Meyers, R.A. (Ed.), Encyclopedia of Complexity and System Science. Springer.

Maurer, H.R., Boerner, D.E., 1998. Optimized and robust experimental design: a non-linear application to EM sounding. Geophysical Journal International 132, 458–468.

Maurer, H.R., Boerner, D.E., Curtis, A., 2000. Design strategies for electromagnetic geophysical surveys. Inverse Problems 16, 1097–1118.

Maurer, H.R., Greenhalgh, S.A., Latzel, S., 2009. Frequency and spatial sampling strategies for crosshole seismic waveform spectral inversion experiments. Geophysics 74, WCC11–WCC21.

Maurer, H., Curtis, A., Boerner, D., 2010. Recent advances in optimized geophysical survey design. Geophysics 75, 75A177–75A194.

Mavko, G.M., Nur, A., 1997. Wave attenuation in partially saturated rocks. Geophysics 44, 161–178.

Mavko, G., Mukerjy, T., Dvorkin, J., 1998. Rock Physics Handbook. Cambridge University Press.

Maxwell, S.C., Rutledge, J., Jones, R., Fehler, M., 2010. Petroleum reservoir characterization using down hole microseismic monitoring. Geophysics 75, 75A129–75A137.

Maz'ya, V., Schmidt, G., 1996. On approximate approximations using Gaussian kernels. IMA Journal of Numerical Analysis 16, 13–29.

Metropolis, N., Rosenbluth, M.N., Rosenbluth, A.W., Teller, A.H., Teller, E., 1953. Equation of state calculations by fast computing machines. The Journal of Chemical Physics 21, 1087–1092.

Monaghan, A.A., McInroy, D.B., Browne, M.A.E., Napier, B.R., 2009. CASSEM work package one – forth geological modelling. BGS Commissioned Report, CR/08/151. British Geological Survey, Edinburgh.

Oldenborger, G., Routh, P., Knoll, M., 2007. Model reliability for 3D electrical resistivity tomography: application of the volume of investigation index to a time-lapse monitoring experiment. Geophysics 72, F167–F175.

Onuma, T., Ohkawa, S., 2009. Detection of surface deformation related with CO_2 injection by DInSAR at InSalah, Algeria. Energy Procedia 1, 2177–2184.

Pham, N.H., Carcione, J.M., Helle, H.B., Ursin, B., 2002. Wave velocities and attenuation of shaley sandstones as a function of pore pressure and partial saturation. Geophysical Prospecting 50, 615–627.

Picotti, S., Carcione, J.M., Rubino, J.G., Santos, J.E., Cavallini, F., 2010. A viscoelastic representation of wave attenuation in porous media. Computers & Geosciences 36, 44–53.

Polson, D., Curtis, A., 2010. Dynamics of uncertainty in geological interpretation. Journal of the Geological Society, London 167, 5–10.

Pride, S., 1994. Governing equations for the coupled electromagnetics and acoustic of porous media. Physical Review B50 (21), 15678–15696.

Pride, S.R., Berryman, J.G., Harris, J.M., 2004. Seismic attenuation due to wave-induced flow. Journal of Geophysical Researches 109, B01201, doi:10.1029/2003JB002639.

Ritchie, J.D., Johnson, H., Browne, M.A.E., Monaghan, A.A., 2003. Late Devonian-Carboniferous tectonic evolution within the Firth of Forth, Midland Valley; as revealed from 2D seismic reflection data. Scottish Journal of Geology 39, 121–134.

Rucci, A., Vasco, D.W., Novali, F., 2010. Fluid pressure arrival-time tomography: estimation and assessment in the presence of inequality constraints with an application to production at the Krechba field, Algeria. Geophysics 75, O39–O55.

Sambridge, M., Mosegaard, K., 2002. Monte Carlo methods in geophysical inverse problems. Reviews of Geophysics 40, 1–29.

Sebastiani, P., Wynn, H.P., 2000. Maximum entropy sampling and optimal Bayesian experimental design. Journal of the Royal Statistical Society, Series B 62, 145–157.

Shannon, C.E., 1948. A mathematical theory of communication. Bell Labs Technical Journal 27, 623–656.

Shi, J., Xue, Z., Durucan, S., 2007. Seismic monitoring and modelling of supercritical CO_2 injection into a water-saturated sandstone: interpretation of P-wave velocity data. International Journal of Greenhouse Gas Control 1, 473–480.

Siggins, A.F., 2006. Velocity-effective stress response of CO_2 saturated sandstones. Exploration Geophysics 37, 60–66.

Stummer, P., Maurer, H., Horstmeyer, H., Green, A.G., 2002a. Optimization of DC resistivity data acquisition: real-time experimental design and a new multi-electrode system. IEEE Transactions on Geoscience and Remote Sensing 40, 2727–2735.

Spikes, K., Mukerji, T., Dvorkin, J., Mavko, G., 2007. Probabilistic seismic inversion based on rock-physics models. Geophysics 72, R87–R97.

Stummer, P., Maurer, H.R., Green, A.G., 2004. Experimental design: electrical resistivity data sets that provide optimum subsurface information. Geophysics 69, 120–139.

Stummer, P., Maurer, H.R., Horstmeyer, H., Green, A.G., 2002b. Optimization of DC resistivity data acquisition: real-time experimental design and a new multi-electrode system. IEEE Transactions on Geoscience and Remote Sensing 40, 2727–2735.

Tarantola, A., 2005. Inverse Problem Theory and Model Parameter Estimation. Society for Applied and Industrial Mathematics, Philadelphia.

Toumelin, E., Torres-Verdín, C., 2008. Object-oriented approach for the pore-scale simulation of DC electrical conductivity of two-phase saturated porous media. Geophysics 73, E67–E79.

Underhill, J.R., Monaghan, A.A., Browne, M.A., 2008. Controls on structural styles, basin development and petroleum prospectivity in the Midland Valley of Scotland. Marine and Petroleum Geology 25, 1000–1022.

van den Berg, J., Curtis, A., Trampert, J., 2003. Optimal nonlinear bayesian experimental design: an application to amplitude versus offset experiments. Geophysical Journal International 155, 411–421.

Verdon, J.P., Kendall, J.M., Maxwell, S.C., 2010. A comparison of passive seismic monitoring of fracture simulation from water and CO_2 injection. Geophysics 75, MA1–MA7.

White, J.E., 1975. Computed seismic speeds and attenuation in rocks with partial gas saturation. Geophysics 40, 224–232.

White, J.E., Mikhaylova, N.G., Lyakhovitskiy, F.M., 1975. Low-frequency seismic waves in fluid saturated layered rocks. Izvestija Academy of Sciences USSR. Physics of the Solid Earth 11, 654–659.

Winterfors, E., Curtis, A., 2008. Numerical detection and reduction of non-uniqueness in nonlinear inverse problems. Inverse Problems 24, 025016.

Xue, Z., Kim, J., Mito, S., Kitamura, K., Matsuoka, T., 2009. Detecting and monitoring CO_2 with P-wave velocity and resistivity from both laboratory- and field scales, SPE 126885. In: The SPE International Conference on CO_2 Capture, Storage, and Utilization, San Diego, California, USA, 2–4 November.

Xue, Z., Lei, X., 2006. Laboratory study of CO_2 migration in water-saturated anisotropic sandstone, based on P-wave velocity imaging. Exploration Geophysics 37, 10–18.

Xue, Z., Ohsumi, T., 2004. Seismic monitoring of CO_2 migration in watersaturated porous sandstone. Exploration Geophysics 35, 25–32.

Yordkayhun, S., Tryggvason, A., Norden, B., Juhlin, C., Bergmann, B., 2009. 3D seismic traveltime tomography imaging of the shallow subsurface at the CO_2 SINK project site, Ketzin, Germany. Geophysics 74, G1–G15.

Zidek, J.V., Sun, W., Le, N.D., 2000. Designing and integrating composite networks for monitoring multivariate Gaussian pollution fields. Applied Statistics 49, 63–79.